Monazite age constraints on the tectono-thermal evolution of the central Appalachian Piedmont

Howell Bosbyshell, Department of Geology and Astronomy, West Chester University, West Chester, Pennsylvania, 19383, U.S.A.
LeeAnn Srogi, Department of Geology and Astronomy, West Chester University, West Chester, Pennsylvania, 19383, U.S.A.
Gale C. Blackmer, Pennsylvania Geological Survey, 3240 Schoolhouse Road, Middletown, PA 17057, U.S.A.

Abstract

The central Appalachian Piedmont lies in the critical juncture between the northern and southern Appalachians, portions of the orogen with distinct middle to late Paleozoic accretionary histories. Orogen-scale compilation maps link the central and southern Appalachians, but until recently, limited geochronological data prevented robust tectonic comparisons between high grade metamorphic rocks in different parts of the orogen. We report the results of in-situ U-Th-total Pb monazite geochronology that date significant deformation and metamorphism as middle Silurian (~425 Ma) through middle Devonian (~385 Ma) and demonstrate the diachronous nature of orogen development. The Rosemont Shear Zone is identified as a major tectonic boundary in southeastern Pennsylvania and northern Delaware separating the rifted Laurentian margin from younger rock units that formed in a magmatic arc setting. The Laurentian margin rocks occur in a series of nappes in which the metamorphic grade decreases from the structurally highest nappe to the lowest. The in situ monazite ages show that maximum temperature in the lowest nappe may have been attained some 15 million years after maximum temperature in the highest nappe. We interpret this to be the result of successive nappe emplacement, with the warmer overriding sheets contributing heat to lower levels. Combining geochronologic and thermobarometric results with the geometry of deformation results in a new picture of the tectonic development of the central Appalachian Piedmont that further links the evolution of the southern and northern Appalachians. For the Laurentian margin rocks, tectonism resulted from the approach and collision of peri-Gondwanan terranes during the Silurian to early Devonian in a dominantly sinistral, transpressive tectonic regime. This portion of the Pennsylvania-Delaware Piedmont inboard of the Rosemont Shear Zone is contiguous with comparable rocks in the southern Appalachians. In contrast, arc-related rock units outboard of the Rosemont Shear Zone experienced primarily thermal metamorphism in the Silurian, while crustal thickening and associated regional metamorphism is middle Devonian in age and likely the result of the accretion of Avalonia during the Acadian orogeny. These arc-related and younger rocks probably originated to the north of their present location as part of the northern Appalachians. They were ultimately emplaced in a right-lateral transcurrent regime sometime after the middle Devonian. Thus, it is in this portion of the central Appalachian Piedmont that the northern and southern Appalachians are joined.

Introduction

The central Appalachian Piedmont lies in the critical juncture between the northern and southern Appalachians, portions of the orogen with distinctly different middle to late Paleozoic accretionary histories. The northern Appalachians are characterized by the latest Silurian to middle Devonian accretion of Avalonia, a period of tectonism which is absent in the southern Appalachians (Hibbard et al., 2010). Geographically, the high-grade metamorphic axis of the central Appalachians is contiguous with the southern Appalachians but separated from the northern Appalachians by the Mesozoic Newark Basin and younger coastal plain sediments (Fig. 1). Orogen-scale compilation maps (Hibbard et al., 2006; Hatcher et al., 2007) link the central and southern Appalachians, but until recently, limited geochronological data prevented robust tectonic comparisons. Here we report the results of in-situ monazite geochronology which demonstrates that significant deformation and metamorphism in the study area is middle Silurian through early Devonian, demonstrating the diachronous nature of terrane accretion in the orogen and linking the evolution of the southern and northern Appalachians.

The power of in situ dating of monazite lies in the ability to relate ages to metamorphic textures and thereby ascribe specific times to stages in the thermo-tectonic evolution of a rock and in turn, an entire orogenic belt. This tool is especially powerful in complex, poly-deformed and metamorphosed rock such as those of the central Appalachian Piedmont. These rocks record multiple periods of metamorphism and deformation as a result of prolonged tectonism from the Middle Ordovician through the Devonian periods. We show the bulk of this tectonism is much younger than previously recognized and is not primarily the product of the Ordovician Taconic orogeny as has long been thought (Crawford and Crawford, 1980; Wagner and Srogi, 1987; Faill, 1997).

This paper concerns the Wissahickon Formation, a classic unit in the central Appalachians that has been the focus of significant work in metamorphic petrology, including early papers on overprinting relationships (Wyckoff, 1952; Amenta, 1974; Crawford and Mark, 1982) and zoning in garnet (Crawford, 1974; 1977). Through in situ dating and microtextural analysis, our paper highlights significant differences in the metamorphic and deformational history between units that have historically been considered part of the Wissahickon Formation. Distinguishing fundamentally different histories in rocks that were once considered to be a single unit has significant implications for orogen scale tectonic interpretations.

Previous Work

Geologic Setting

The central Appalachian Piedmont in Pennsylvania is underlain by Mesoproterozoic gneiss and latest Neoproterozoic to early Paleozoic metasedimentary cover rock (Fig. 1). The Laurentian margin metasedimentary rocks preserve a history of rifting during the breakup of super-continent Rodinia, the formation of a stable margin carbonate platform, and the eventual foundering of this platform during Paleozoic orogenesis (Faill, 1997; Wise and Ganis, 2009). These rocks occur in a series of gneiss-cored nappes or thrust sheets (Wise and Ganis, 2009) which are cut by younger, northeast trending, transcurrent shear zones, the Pleasant Grove-Huntingdon Valley (PGHV) and Rosemont (RSZ) shear zones (Valentino et al., 1994, 1995). External nappes (northwest of the PGHV) experienced metamorphism no higher than greenschist facies during Paleozoic orogenesis (Sutter et al., 1980; Crawford and Hoersch, 1984; Pyle, 2006).

We focus on rocks from the Embreeville Thrust (Fig. 1) southeast to the coastal plain onlap, which occur in two crustal blocks that comprise the high-grade metamorphic core of the orogen. The RSZ separates rift-related Laurentian margin rocks to the northwest (Bosbyshell et al., 2014), from the Ordovician-aged metavolcanic/magmatic arc rocks, associated lower-Paleozoic metasedimentary rock, and Silurian-aged intrusive rock which underlie southeastern-most Pennsylvania and northern Delaware (Crawford and Crawford, 1980; Wagner and Srogi, 1987; Aleinikoff et al., 2006). These rocks contain evidence for multiple episodes of amphibolite to granulite facies metamorphism (Crawford and Mark, 1982; Wagner and Srogi, 1987; Alcock and Wagner, 1995; Bosbyshell et al., 1999) and preserve a complex structural history, the details of which have been debated for more than a century (Bliss and Jonas, 1916; Knopf and Jonas, 1923; McKinstry, 1961, Mackin, 1962; Wise, 1970; Wiswall, 1990; Alcock, 1994; Valentino, et al., 1994; Alcock and Wagner, 1995).

We follow the usage of Bosbyshell et al. (2013, 2014) who introduced the name West Grove Metamorphic Suite to refer to rock between the Embreeville Thrust and RSZ which is shown on many published maps as "Glenarm Wissahickon" (Faill and Wiswall, 1994; Blackmer, 2004a, 2004b, 2005; Wiswall, 2005; Blackmer et al., 2010) or, in Delaware, "Wissahickon Formation" (Plank et al., 2000; Schenck et al., 2000). The Wissahickon Formation, *sensu stricto,* (Bascom et al., 1909; Bascom and Stose, 1932, 1938) is named for its type locality in exposures along Wissahickon Creek in Philadelphia, Pa. However, differences between the Wissahickon Formation east of the RSZ and rock mapped as "Glenarm Wissahickon" west of the RSZ (Fig. 1) have long been recognized (e.g. Faill and MacLachlan, 1989; Faill and Wiswall, 1994) and are more fully documented in this paper. The West Grove Metamorphic Suite consists of metasedimentary units, Doe Run Schist and Mt. Cuba Gneiss, and geochemically distinct amphibolites; the Kennett Square Amphibolite is similar to mid-ocean ridge basalt (MORB) and the White Clay Creek Amphibolite is similar to within-plate basalt (Smith and Barnes, 1994, 2004; Plank et al., 2001).

Structural Geology

The structural framework adopted in this paper is based on relatively recent mapping by the Pennsylvania and Delaware geological surveys (Schenck et al., 2000; Blackmer, 2004a, 2004b, 2005; Wiswall, 2005; Blackmer et al., 2010). The Embreeville Thrust (Fig. 1) is the lowest structure in a series of nappes composed of basement gneiss and metasedimentary cover. From structurally lowest to highest, these include the West Chester nappe, Avondale nappe, and Mill Creek (Hockessin-Yorklyn) anticline (Schenck et al., 2000). The gneiss is thought to be similar to Mesoproterozoic basement gneiss to the south in Maryland and is known as Baltimore Gneiss (Bascom et al., 1909; Bascom and Stose, 1932), although sparse geochronological data indicate that gneiss within the Avondale nappe may be lower Paleozoic and not Mesoproterozoic in age (Grauert et al., 1973, 1974; Bosbyshell et al., 2006). The metasedimentary cover sequence in the nappes consists of the probable early Cambrian-aged Glenarm Group and West Grove Metamorphic Suite (Bosbyshell et al., 2013; 2014).

The dominant foliation in this area, the regional S_2 foliation (Blackmer 2004a, 2004b, Wiswall, 2005), dips shallowly to moderately to the southeast (Figs. 2A and D). This foliation is axial planar to overturned to recumbent outcrop scale folds, which exhibit top to the northwest asymmetry (Alcock, 1994; Blackmer, 2004a) and is parallel to the foliation in thrust-sense shear zones at the base of the nappes described above (Bosbyshell et al., 2006). The S_2 foliation, therefore, likely formed as a result of thrust emplacement. Rootless isoclinal folds, visible in outcrop and thin section, now parallel to the S_2 foliation, preserve an older, S_1 fabric. This older foliation is present at the outcrop scale in a few locations (Blackmer, 2004a) where it is steeply dipping to sub-vertical. The dominant S_2 foliation generally trends approximately 065 to 075; this trend becomes more northerly in the Woodville structure, which Blackmer (2004a) interprets as a sheath fold. The S_2 foliation is deformed by upright folds, especially in the northwestern- and southeastern-most rocks (Alcock, 1994; Blackmer, 2004a; Wiswall, 2005). This upright folding is attributed to younger, transpressive deformation in the PGHV and Rosemont shear zones (Valentino et al., 1994, 1995).

This structural framework differs somewhat with earlier work of Alcock (1994) and Alcock and Wagner (1995), who postulate the emplacement of the WGMS as large thrust sheet prior to nappe stage folding. Their interpretation results in a markedly different stratigraphy within metasedimentary rock and structural geometry in the area of the Woodville structure. These differences are discussed by Blackmer (2004a, 2004c) and Bosbyshell et al. (2014).

The nappes and associated southeast dipping fabrics are truncated to the southeast by the steeply dipping (Fig. 2B) RSZ (Valentino et al., 1995; Bosbyshell 2005a, 2005b), the western boundary of Ordovician-aged (475 to 485 Ma; Aleinikoff, et al., 2006) granulite facies metaigneous rock of the Wilmington Complex (Wagner and Srogi, 1987), and other arc-related metasedimentary and metavolcanic rock of the Wissahickon Formation (Fig. 1).

Detailed structural analysis in the Wissahickon Formation metasedimentary rocks southeast of the RSZ has been conducted by Amenta (1974), Tearpock and Bischke (1980) and Bosbyshell (2001, 2008). These studies describe similar deformational histories, involving five recognizable stages. Different generations of structures are preserved to varying degrees at the map or even outcrop scale, depending on local metamorphic history (Amenta, 1974; Bosbyshell, 2001). The oldest deformation is an early foliation present in the hinges of S_2 folds and as transposed F_1 hinges rarely preserved within the S_2 schistosity. The regional schistosity is the S_2 foliation, which, though affected by younger folds, generally dips moderately to steeply to the northwest. S_2 is axial planar to F_2 isoclinal folds and is in turn folded by F_3 folds. F_3 folds are close to tight, upright to recumbent, and are associated with a variably developed sub-vertical to moderately northwest-dipping axial planar foliation. In much of the area, S_2 is reoriented by F_3 folds and the dominant foliation is an S_2/S_3 composite (Fig. 2C). Fabrics associated with the RSZ (S_4) are younger than F_3 folds (Amenta, 1974; Bosbyshell, 2001). The youngest ductile fabrics include sub-horizontal crenulation (S_5) and associated outcrop scale open folds which are variably developed throughout the area (Amenta, 1974; Tearpock and Bischke, 1980; Valentino and Gates, 2001; Bosbyshell, 2008).

Gneissic fabrics in metaigneous rock of the Wilmington Complex are sub-vertical to steeply northwest dipping along the northwest margin of the Complex, approaching the RSZ, and dip moderately to the northwest elsewhere (Schenck et al., 2000). The pattern is similar to that in the Wissahickon Formation to the northeast of the Wilmington Complex and contrasts with the shallow to moderate southeast dips in rocks to the northwest.

Metamorphic History

The metamorphic history of the WGMS has been studied by Alcock (1989, 1994), who estimated peak metamorphic conditions in the Doe Run Schist to be 575 ±50 °C at 850 ± 100 MPa. In the Mt. Cuba Gneiss, Plank (1989) found that metamorphic conditions varied from 600 ±50 °C at 500 to 600 MPa in southeastern-most Pennsylvania to 750 ±50 °C at 600 to 700 MPa nearest the Wilmington Complex in Delaware. Alcock (1989, 1994) and Alcock and Wagner (1995) report similar temperatures, at slightly lower pressure, 700 ± 50 °C at 500 ± 100 MPa for peak conditions in the Mt. Cuba Gneiss. TIMS (424.9 ± 0.4 Ma) and SHRIMP (426 ± 3 Ma) U-Pb monazite results indicate that high temperature metamorphism in the Mt. Cuba Gneiss is Silurian in age (Aleinikoff et al., 2006). Alcock (1989) and Blackmer (2004a, 2004b), and results presented below, indicate that formation of the dominant S_2 foliation in both the Doe Run Schist and Mt. Cuba Gneiss is broadly synchronous with high temperature metamorphism.

Two periods of metamorphism are documented in the Wissahickon Formation east of the RSZ: early high temperature – low to moderate pressure assemblages are variably overprinted by a second period of higher pressure metamorphism, 650 ±50 °C, 700 ±100 MPa (Crawford and Mark, 1982; Bosbyshell et al., 1999; Bosbyshell, 2001). The temperatures associated with the early metamorphism vary from west to east. Nearest the Wilmington Complex, peak conditions were likely in excess of 700 °C at 500 ±100 MPa while less than 10 km to the east, andalusite was part of the early assemblage, implying temperatures of approximately 500 °C (Bosbyshell et al., 1999). Electron microprobe Th-U-total Pb monazite ages (Bosbyshell, 2001; Pyle et al., 2006) constrain the early metamorphism to be Silurian in age (~430 Ma), similar in age to granulite facies metamorphism in the Wilmington Complex and plutonism in both the Wilmington Complex and Wissahickon Formation (Aleinikoff et al., 2006; Bosbyshell et al., 2005). The higher pressure overprint occurred during the Devonian (~380 Ma, Bosbyshell et al., 1998; Bosbyshell, 2001; Pyle et al., 2006).

Analysis of metamorphism in the type section of the Wissahickon Formation and the adjacent area has not been undertaken since the studies of Amenta (1974) and Crawford (1974, 1977), although Bosbyshell (2008) describes metamorphism in the Philadelphia quadrangle to the south. Crawford (1977) estimated peak conditions in the type section to be 600 ±50 °C, 750 ±100 MPa. The results presented below indicate that the early, high-T low-P metamorphism is largely absent in the type section; the main period of metamorphism preserved there reflects the younger, higher pressure period of metamorphism.

Methods

Prior to in-situ electron probe microanalysis (EPMA), key monazite grains were selected using the FEI Quanta scanning electron microscope and the Oxford Instruments energy dispersive spectroscopy system (EDS) and INCA software in the Center for Microanalysis Imaging and Training (CMIRT) at West Chester University of Pennsylvania. Please see the online supplement for an account of the procedure that was utilized.

The EPMA monazite results described below were acquired over several years at two microprobe facilities. Five samples – DR-1, DR-3, MC-1, MC-2 and WF-2 –were analyzed using the Cameca Ultrachron microprobe at the University of Massachusetts, Amherst following the procedures outlined by Williams et al. (2006) and Dumond et al. (2008). Geographic coordinates and original sample numbers are listed in Table 1. In brief, background values for Th, U, Pb, and K were determined from regression of high-resolution wavelength scans (e.g., Williams et al., 2006; Jercinovic et al., 2008), while background values for all other elements were based on a two-point linear interpolation. At least one background regression was carried out in each homogeneous compositional domain, as determined from compositional mapping. The 5 to 10 measurements made within a compositional domain were corrected to the same background and used to calculate a single date and error estimate for each compositional domain. Two samples, DR-2 and WF-1, were analyzed using the Cameca SX-100 microprobe at Rensselaer Polytechnic Institute utilizing analytical and background acquisition techniques described by Spear et al. (2008) and Pyle et al. (2005). The same consistency standard, Moacyr Brazilian pegmatite monazite, was utilized in both laboratories to provide a qualitative assessment of accuracy during each analytical session (Williams et al., 2006). The Moacyr monazite standard has weighted mean ages of 506 ± 1 (2σ, MSWD = 0.6) for 208Pb/232Th, 506.7 ± 0.8 Ma (2σ, MSWD = 0.83) for 207Pb/235U, and 515.2 ± 0.6 Ma (2σ, MSWD = 0.36) for 206Pb/238U obtained by isotope dilution–thermal ionization mass spectrometry (ID-TIMS) at the Geological Survey of Canada (W.J. Davis, 2010, personal communication with M.L. Williams).

Metamorphic conditions were estimated using equilibrium assemblage diagrams and garnet isopleths calculated with the software Theriak-Domino (de Capitani and Petrakakis, 2010). H_2O content for use in equilibrium assemblage models was chosen by calculating binary diagrams in H, at different pressures, to estimate the abundance of H_2O required to model the observed assemblage. Oxygen was allowed to vary according to mineral stoichiometry. Calculations were performed using the THERMOCALC database with the garnet solution model tc325 (Powell and Holland 1994; Powell et al. 1998; White, RW, Powell, R & Holland, 2007).

In addition to the thermodynamic database and solution models, Theriak-Domino results depend on the bulk rock composition used in the calculation. Bulk rock compositions were determined by two methods. The composition of samples MC-1 and DR-2 was determined by X-ray fluorescence spectrometry (XRF) performed by Activation Labs on crushed rock from the same samples from which thin sections were prepared. Whole rock analysis of sample WF-1 was obtained by EDS analysis of a thin section performed at the CMIRT of West Chester University. Details of the procedure and a comparison of XRF whole rock results with results obtained using EDS scans of thin sections is provided in Appendix 1.

We note that regardless of the technique used to determine bulk rock composition, it is difficult to know the true effective bulk composition, i.e., the composition of the volume of rock which attains chemical equilibrium, for use in modeling. The effective bulk composition likely varies through time depending on such factors as metamorphic temperature (as this effects diffusion length scales), the presence and composition of a fluid phase, the removal or introduction of a melt phase, and the sequestration of atoms within growing porphyroblasts (e.g., Evans, 2004; Tinkham and Ghent, 2005). In layered metamorphic rocks which are anisotropic and heterogeneous at the mm.-scale, the composition of a thin section may more closely approximate the effective bulk composition than a larger volume of rock. Accounting for these factors is not the purpose of the present investigation. While recognizing that such coincidence may be fortuitous, we suggest that if the input bulk composition is successful in modeling the measured composition of garnet and the observed mineral assemblage, then that composition is a reasonable approximation of the effective bulk composition.

X-ray compositional maps of garnet and garnet analyses were obtained by EPMA using the Cameca SX-50 at the University of Massachusetts and by EDS analysis at West Chester University. The EDS system is known to yield less than ideal stoichiometry for Si and Al; however, calculated garnet end member proportions are indistinguishable from those obtained by EMPA. A comparison of garnet end members calculated from EPMA and EDS analysis of the same garnet is provided in Appendix 2.

Metamorphism

In this section we describe metamorphic mineral assemblages and the sequence of deformation and metamorphism in the West Grove Metamorphic Suite and Wissahickon Formation, including detailed petrographic description and qualitative and quantitative pressure and temperature estimates of samples selected for monazite geochronology.

West Grove Metamorphic Suite

Doe Run Schist. The Doe Run Schist, which occurs above the Embreeville Thrust in the West Chester nappe (Fig. 1), is coarse-grained schist, primarily composed of quartz, plagioclase, muscovite, biotite, and garnet. Staurolite and kyanite are common and sillimanite is present in some samples. Staurolite and garnet are quite coarse, commonly having centimeter-scale dimensions. The dominant foliation throughout the Doe Run Schist is the regional S_2 foliation and is defined by aligned biotite and muscovite and mm-scale interlayering of quartzo-feldspathic and micaceous domains, including relatively uncommon biotite + sillimanite domains. S_2 foliation wraps around garnet and staurolite porphyroblasts, but staurolite also occurs parallel to S_2 foliation and in some samples late garnet overgrows this foliation. Many rocks contain an older foliation preserved in microlithons or as inclusion trails in garnet and staurolite. In some rocks of the Doe Run Schist, especially near the trace of the Embreeville Fault, staurolite is replaced by sericite and chlorite and garnet is rimmed by chlorite (Moore et al., 2007).

Two key samples, DR-1 and DR-2, that exhibit textural evidence for the high temperature breakdown of staurolite to sillimanite and garnet were selected for monazite analysis. Staurolite porphyroblasts are rimmed by fine sillimanite and there is evidence for episodic garnet growth in response to staurolite formation and breakdown. Sample DR-1 contains two generations of garnet: early small euhedral garnet that is included within staurolite and younger small, elongate to euhedral garnet that is synchronous with or younger than the dominant foliation (Bukeavich et al., 2006). Clusters of this texturally younger garnet are associated with fine sillimanite along embayed rims of staurolite, indicating that the younger garnet likely formed at the expense of staurolite (Fig. 3A). In DR-2. the S_2 foliation is cut by younger shear bands, perhaps owing to its location beneath the Street Road Fault, which cause the foliation to envelop coarse (up to 5 mm in the longest dimension) subhedral garnet and staurolite, which is elongate parallel to foliation (Fig. 3B). Garnet exhibits relatively inclusion poor inner cores, outer cores with foliation-parallel inclusion trails and distinct, inclusion-free rims.

Well preserved zoning in garnet porphyroblasts in DR-2 allow detailed reconstruction of the metamorphic history. X-ray composition maps of garnet from DR-2 are shown in Figure 4A. The maps show Ca concentration decreasing from core to rim, with a sharp step to lower concentration in the rim. Mg concentration increases from core to rim, while Mn concentration decreases away from the core but increases in the rim. Figures 4B and 4C are based on an equilibrium assemblage diagram for sample DR-2, calculated using the software Theriak-Domino (de Capitani and Petrakakis, 2010). The bulk rock composition used in calculations is given in Table 2; garnet analysis is in Table 3. The shaded area indicates fields where staurolite is part of the stable assemblage; figure 4B shows contours of grossular component while 4C shows molar garnet isopleths. Garnet zoning requires a pressure-temperature history along a path of decreasing grossular component (arrow in Fig. 4B and C). The amount of garnet in the assemblage decreases as staurolite grows but increases sharply, at lower Ca-content, at the high temperature stability limit of staurolite. Thus, the low-Ca portion of the garnet rim (Fig. 3) corresponds to the highest temperature history of the rock. Isopleths of this garnet composition intersect at 700 °C and 500 MPa. Under these conditions the diagram indicates that melt may be present, consistent with textures that suggest a small amount of leucosome is present in the rock. A small increase in Ca in garnet rims may indicate an increment of garnet growth as a result of a slight increase in pressure or during isobaric cooling.

Mt. Cuba Gneiss. The Mt. Cuba Gneiss occurs above the Street Road Fault in the Avondale nappe and within the structurally highest Mill Creek nappe (Fig. 1). It is composed of psammitic gneiss with subordinate pelitic gneiss and pegmatite. The highest grade metamorphic rocks occur in the Mill Creek nappe where the rock is metatexite and contains considerable evidence for partial melting. Centimeter- to decimeter-scale granitic leucosome containing perthitic alkali feldspar, plagioclase and quartz is common; micrometer-scale leucosome with Ba-rich alkali feldspar, plagioclase and quartz occurs along mesosome grain boundaries. Melanosome is rich in garnet and biotite, but neither cordierite nor orthopyroxene is observed. Sillimanite is present in pelitic lithologies but is only rarely preserved as aligned inclusions within plagioclase in psammitic rock. Some leucosome contains biotite parallel to mesosome foliation; other leucosome contains randomly-oriented biotite, which suggests syn- to post-kinematic partial melting with respect to foliation formation. Given the presence of perthitic feldspar and sillimanite, maximum temperature likely exceeded 750 °C, but remained below the temperature of the first appearance of orthopyroxene, at pressures above the stability of cordierite.

Rocks of the WGMS in the Avondale nappe contain the assemblage quartz, plagioclase, garnet, biotite, sillimanite, and ilmenite, with or without staurolite; a small amount of texturally late muscovite is present in some rocks. Monazite was analyzed in one sample which contains staurolite, MC-1, and one which does not, MC-2. In both rocks, S_2 is defined by aligned sillimanite and biotite and mm-scale quartzo-feldspathic domains. In MC-1, anhedral staurolite grains occur parallel to the dominant foliation and contains inclusions of foliation-parallel fibrolitic sillimanite, but are also surrounded by and possibly replaced by nematoblastic and fibrolitic sillimanite (Fig. 5A). Kyanite occurs as small crystals which overprint sillimanite (Fig. 5B). The dominant foliation wraps garnet, but subhedral to euhedral rims on some garnet grains cut foliation.

Temperature and pressure of metamorphism in sample MC-1 were estimated using an equilibrium assemblage diagram calculated with the bulk composition in Table 2 (Fig. 6). Garnet in Mt. Cuba Gneiss shows very little major element zoning, with the exception of grossular component. Ca content decreases in the rim, but increases in a narrow zone in the outermost rim (Fig. 5C). The lack of zoning in the garnet core is likely the result of diffusional homogenization during high temperature metamorphism, so that the original composition of the garnet interior has been modified and may not reflect an equilibrium composition. Isopleths of the composition of the garnet core do not cluster in P-T space. A lack on complete equilibration is further indicated by the presence of staurolite and leucocratic segregation, indicating a degree of partial melting. On equilibrium assemblage diagrams (Fig. 7), the first liquid does not appear until temperature exceeds the stability of staurolite. The observed assemblage, without staurolite, is stable in a field that spans 700 °C (the first appearance of liquid) to 800 °C (the maximum temperature of biotite stability), at pressure between 550 MPa (the limit of cordierite stability) to 800 MPa (the first appearance of rutile). The estimate can further refined by noting that biotite is abundant in MC-1, but modeled biotite abundance decreases sharply as temperature increases. The isopleth corresponding to the measured Ca content of the garnet interior (X_{Grs} = 0.05), the component least affected by diffusion, intersects the stability field of the peak assemblage. We estimate that peak metamorphic conditions in the Mt. Cuba Gneiss of the Avondale nappe were approximately 725 °C at 600 GPa.

Porphyroblast-fabric relationships described above demonstrate that deformation and amphibolite facies metamorphism throughout the WGMS are synchronous. In both the Doe Run Schist and Mt. Cuba Gneiss, staurolite occurs parallel to the S_2 foliation, but is also wrapped by foliation. Mutually cross-cutting relations between foliation and garnet are also present: S_2 foliation wraps around garnet, but late garnet growth also crosscuts foliation, suggesting that high temperatures likely persisted after deformation ceased.

Wissahickon Formation.

The metamorphic grade in the type section of the Wissahickon Formation increases from staurolite-bearing rock in the north, through kyanite grade rock, to sillimanite-bearing rock in the south (Crawford, 1987). We collected samples along the length of Wissahickon Creek, from the staurolite zone to the sillimanite zone, and prepared major element x-ray composition maps of garnet from 12 thin sections. With the exception of one sample, all garnet shows relatively simple zoning, indicative of a single stage of metamorphism. In sillimanite zone rocks, Fe, Ca, and Mg show little zoning while Mn shows an increase at the garnet rim (Fig. 7A). Garnet in samples from the kyanite + staurolite zone show little zoning in Fe and Mg, but do exhibit core to rim decreases in Ca and Mn. Mn shows a slight increase at the rim and Ca maps exhibit a low-

Ca rim (Fig. 7B). Similar zoning is also present in garnet at the northern end of the transect in rocks which contain staurolite and little to no kyanite.

The exception is sample WF-1, in which garnet crystals exhibit a small very low-Ca, high-Mn core (Fig. 7C). WF-1 was collected approximately 200 meters south of the contact with Mesoproterozoic gneiss of the West Chester nappe at the contact with a 15 meter thick dike of granodioritic gneiss. The sample (Fig. 8A) contains the assemblage muscovite + biotite + garnet + quartz + plagioclase + ilmenite with minor staurolite and kyanite. The dominant foliation, S_2/S_3 composite, is defined by aligned muscovite with some biotite and by mm-scale compositional layering. In addition to being a fabric defining phase, biotite also occurs as porphyroblasts up to 0.5 mm in longest dimension which may be pre-kinematic with respect to the dominant foliation. The S_2/S_3 foliation is crenulated and cut by shear bands, resulting from deformation in the Rosemont shear zone. This younger deformation likely reactivated the dominant foliation, obscuring the relative timing of porphyroblast growth and fabric formation. Garnet porphyroblasts are subhedral and up to 2 mm in diameter and are wrapped by the reactivated S_2 foliation.

Metamorphic conditions in sample WF-1 were also estimated using an equilibrium assemblage diagram and garnet isopleth thermobarometry (Fig. 9). Isopleths reflecting the composition of the outer core of the garnet shown in Figure 7A intersect at approximately 600 °C and 700 MPa. A very small amount of staurolite is present in the sample, but staurolite-bearing assemblages do not appear on the diagram in Figure 9. Model calculations (not shown) suggest that this is likely the result of the abundance of K or Fe in the bulk composition; staurolite appears in assemblages modeled with lower K or greater Fe in the input bulk composition. Very minor kyanite is also present in the rock. Kyanite does not become part of the modeled assemblage until temperatures slightly higher than the intersection of garnet isopleths, indicating that the maximum metamorphic temperature may be near 650 °C.

The deformation and metamorphism in the Wissahickon Formation, midway between the Wilmington Complex and the type section, is well illustrated in sample WF-2 (Fig. 8B). The rock here exhibits evidence of the two-stage history described above (Crawford and Mark, 1982; Bosbyshell et al., 1999; Bosbyshell, 2001). Pelitic schist is medium to coarse grained and is composed of quartz, biotite, muscovite, plagioclase, garnet, staurolite, and kyanite. Sillimanite is present as very fine acicular inclusions in garnet and muscovite. Andalusite is part of the early assemblage in these rocks; unaltered andalusite has been found (Gordon, 1922; Wyckoff, 1952; Heyl, 1980; Hess, 1981), but is very rare. Nodules consisting of kyanite, muscovite, and, in some rocks, staurolite, are common and are interpreted as pseudomorphs after andalusite (Crawford and Mark, 1982; Bosbyshell et al., 1999; Bosbyshell, 2001).

The garnet at right in Figure 8B is shown in the element maps in Figure 7D, which illustrate the two stage metamorphic history. This sample contains the kyanite-bearing assemblage, but sillimanite inclusions are present in garnet. The small euhedral core, which is particularly evident in the Ca map, is interpreted to have grown during the early low-pressure metamorphism, while the high-Ca overgrowth formed during younger higher pressure metamorphism. Inclusion trails in garnet are essentially parallel to the external foliation, but wrap around the small, euhedral, relatively inclusion-free garnet core. Garnet in this rock is very Mn-rich ($Sps_{0.15}$ to $Sps_{0.25}$), a composition that is difficult to model effectively. P-T conditions of the early metamorphism are constrained by the inferred presence of andalusite; the younger assemblage represents conditions in the stability field of staurolite + kyanite. Traditional thermobarometry (Grt-Bt; GASP) on similar rock yielded results of 600 ± 50 °C and 750 ± 100 MPa (Bosbyshell, 2001), consistent with the presence of staurolite and kyanite.

Monazite Geochronology

Doe Run Schist

Twenty-four monazite grains were analyzed in three samples of Doe Run Schist. The results are presented in Table 4 and Figure 10A. All errors reported below are 2σ.

The five monazite grains analyzed in DR-1 exhibit patchy irregular zoning in Th but little zoning in U or Y. The core of one grain, included within a large matrix biotite, gives an age of 454 ± 8.5 Ma, significantly older than the other analyzed grains; another, partially included in ilmenite, is significantly younger, 357 ± 12 Ma, than the others. With the exception of a high-Th core in one grain, which yields an age of 429 ± 6 Ma, there is no statistically distinguishable age difference in domains of varying Th content in the remaining monazite grains. The weighted average age of the five different compositional domains is 409 ± 7 Ma (M.S.W.D. = 2.6)

Monazite in sample DR-3 also exhibits zoning in Th with no discernible age difference in different compositional domains. Many monazite grains in this sample are partially replaced by apatite. The ages of four of the six grains analyzed are statistically indistinguishable and give an average of 416 ± 7.5 Ma (M.S.W.D. = 5.2). A low-Th domain in an inclusion in staurolite, yielded 425.5 ± 8 Ma and a low-Th core a matrix grain is even older, 455 ± 8 Ma.

Thirteen monazite grains were examined in DR-2; three age domains, based on composition and texture, are present. Nine analyses of small, irregularly shaped, low-Th cores yield an average of 491 ± 9 Ma (M.S.W.D. = 0.9). Apart from these small cores, the interiors of most grains are variably zoned in Th, but exhibit little zoning in U and Y. An average age of 453 ± 4 Ma (M.S.W.D. = 0.9) was obtained from 31 individual analyses in these interior domains, or approximately three analyses per grain. High Th, low Y rims are present on some, but not all, monazite grains analyzed in this sample. Eight spot analyses of these rims give an average age of 408 ± 4.5 Ma (M.S.W.D. = 2.4).

Mt. Cuba Gneiss

In the Mt. Cuba Gneiss, monazite was analyzed in MC-1, a sample from the hanging wall, just south of the trace of the Street Road fault, and MC-2, from below the Mill Creek nappe. In MC-1, 33 compositional domains in 10 grains were analyzed and in MC-2, we analyzed 15 compositional domains in seven grains. EPMA results from MC-1 reveal complex zoning in monazite and, the presence of two age populations (Fig. 10B): 419 ± 3.5 Ma (M.S.W.D. = 1.3) and 438 ± 4 Ma (M.S.W.D. = 1.6). Both inclusions and matrix grains contain compositional domains which yield both older and younger ages and there is no apparent relationship between age and composition. High Th rims on one grain yield a Devonian age, 365 ± 9 Ma.

Monazite in MC-2 also exhibits complex zoning patterns. Many grains contain high-Th cores which are rimmed by low-Th, high-Y domains and several grains contain low-Th inner cores. One low-Th inner core yields an age of 453 ± 9 Ma; cores and interior domains range in age from 424 ± 7 to 434 ±6, with a weighted average of 429 ± 6 Ma (M.S.W.D. = 0.39); rims and outer core domains yield a weighted average of 414 ± 5 Ma (M.S.W.D. = 0.36).

Wissahickon Formation

Nine monazite grains were analyzed in sample WF-1 and three were analyzed in sample WF-2; the results are shown in Figure 10C. The monazite grains examined in WF-1 are matrix grains, with the long dimension parallel to foliation. All exhibit zoning in Th and Y, but with one exception, an older core (428 ± 4.5 Ma) described below, distinct age domains are not resolvable. Eight of these grains give an average of 390 ± 4.5 Ma (M.S.W.D. = 4.7). One additional grain, m20, which occurs in a pressure shadow adjacent to garnet, gives an age of 414 ± 8 Ma.

Monazite in sample WF-2 is characterized by distinct core-rim zoning. All monazite examined have high-U rims which surround interiors exhibiting patchy irregular zoning in Th and Y. The irregularly zoned interiors of four grains yield an average age of 431 ± 3 Ma (M.S.W.D. = 0.59). Rim domains span 425 ± 4 Ma to 404 ± 6 Ma (Fig. 12B).

Discussion

Interpretation of monazite ages.

Doe Run Schist. Monazite results in the Doe Run Schist demonstrate that peak metamorphic temperatures could not have been attained prior to the early Devonian, at approximately 409 Ma. In DR-1, monazite of this age is typically elongate parallel to foliation and one analyzed grain exhibits asymmetry (Fig. 11A), suggesting syntectonic monazite growth at this time. Small euhedral garnet crystals, interpreted to have grown as a result of high-temperature breakdown of staurolite (Fig. 3) appear texturally younger that foliation-forming mica. Thus, if foliation-parallel monazite formed at or before 409 Ma, the euhedral garnet and attainment of maximum metamorphic temperatures can be no older than this. In sample DR-2, the age of high-Th low-Y rims monazite rims is also ~409 Ma (408 ± 4.5). As illustrated in Figure 11B, monazite inclusions in the low-Ca rims on garnet in DR-2, described above, exhibit these high-Th, low-Y rim domains. The growth of low-Ca rims on garnet, which are the product of maximum metamorphic temperatures, can be no older than the monazite rims. Because Y preferentially fractionates into garnet, the low-Y character of the monazite rims is consistent with monazite formed during garnet growth (Pyle et al., 2001). Thus, the high-Th low-Y domains likely record the time of peak metamorphism in this sample.

Monazite results from the third Doe Run Schist sample, DR-3, offer less direct constraints, but are consistent with those described above. Foliation-parallel matrix monazite in

DR-3 give an average 416 ± 8 Ma, which may constrain the age of deformation in this rock. The growth of staurolite in this rock must be younger than 428 Ma, the age of a monazite inclusion.

Older cores in monazite, which cluster around 455 Ma, are present in all samples of Doe Run Schist that we analyzed. The significance of these ages is difficult to interpret because there is generally no direct textural context to which monazite growth can be related. One grain in sample DR-2 (m311) is an inclusion in staurolite within a microlithon (Fig. 11C), which preserves an older foliation (F_1?) oriented at a high angle to the dominant foliation in the rock. This grain is elongate parallel to foliation in the microlithons and yielded only the older age; younger age domains were not present. Thus, this older generation of monazite in the Doe Run Schist likely corresponds to formation of an older foliation and an earlier period of metamorphism.

Mt. Cuba Gneiss. Two age domains are present in MC-1, 419 ± 3.5 Ma and 438 ± 4 Ma. The older ages typically occur in cores, but there is no consistent compositional variation between or within the two age groups. Monazite grains that yield the younger age are present as inclusions in garnet, staurolite, and plagioclase. Thus, the monazite results indicate that peak metamorphism can be no older than 419 Ma. Monazite in MC-2 exhibits distinct core-rim zoning in Th and Y, which are also distinct age domains. Seven rim domains average 414 ± 5 Ma; six cores average 429 ± 6 Ma. As in MC-1, monazite with the younger rims is present as inclusions in poikiloblastic garnet, providing a constraint on the maximum age of garnet growth in this rock.

In MC-1, one grain (m204) occurs along a grain boundary between plagioclase and garnet and is partially included in both phases (Fig. 12). The garnet is rimmed by Al_2SiO_5 along the grain boundary it shares with plagioclase. The aluminosilicate could be either kyanite or sillimanite, the relationship with plagioclase and garnet suggests that it formed by reaction involving these phases (the GASP geobarometer, 3An = Grs + $2Al_2SiO_5$ + Qtz). The high-U portion of the monazite yields the older age while the remainder of the grain gives the younger age; therefore the garnet rim and plagioclase with which it is in contact can be no older than 419 Ma. The very narrow high-Th rim on the upper right of the monazite crystal (Fig. 12) yields the Devonian age, 365 ± 15 Ma. Since both grain boundary reactions (formation of Al_2SiO_5 and monazite) were likely mitigated by grain-boundary fluids (Williams et al., 2011), it is reasonable to assume that the reactions are broadly synchronous. If so, the monazite age could constrain the timing of formation of the narrow high-Ca rim on garnet and the kyanite-grade metamorphism modeled using garnet isopleths (Fig. 6).

A Silurian age for monazite in the Mt. Cuba Gneiss in the Mill Creek nappe (SHRIMP and TIMS, 426 ± 3 Ma and 424.9 ± 0.4 Ma, respectively) was determined by Aleinikoff et al. (2006). These results were obtained using mineral separates, so uncertainty exists regarding the timing of monazite growth relative to deformation and metamorphism. To address this, we examined the textural occurrence of monazite in six oriented thin sections prepared from a sample collected immediately adjacent to Aleinikoff et al.'s (2006) sample 44069. Four are vertical sections cut perpendicular to strike; two are vertical sections parallel to strike. Utilizing the image analysis capabilities of the Oxford INCA software program Feature, we determined the aspect ratio and orientation of the long dimension of all monazite grains in each thin section. The results presented in Figure 13 indicate that the majority of monazite grains are parallel to the plane of foliation. It is possible that monazite growth predates deformation and that monazite grains rotated to the present orientation, however, the consistent foliation parallel orientation indicates that they are broadly syntectonic. The modelling of Spear and Pyle (2010) indicates that monazite growth is unlikely at temperatures above the solidus. Leucosome in this rock is present in a deformed and undeformed state, indicating that at least some deformation is synchronous with attainment of peak temperatures. Thus, the 425 Ma result of Aleinikoff et al. (2006) most likely corresponds to monazite growth during deformation and prograde metamorphism and is the maximum age of partial melting in the Mt. Cuba Gneiss of the Mill Creek nappe.

Wissahickon Formation. Sample WF-1 comes from the contact between the Wissahickon Formation and a small dike of granodioritic gneiss. The age of the igneous protolith of this gneiss is uncertain, but a larger intrusion of similar composition, the Springfield Granodiorite (Fig. 1), yielded a U-Pb zircon age of 427 ± 3 Ma (Bosbyshell et al., 2005). This is essentially the same as the age of the oldest monazite core in WF-1, 428 ± 4.5 Ma (Fig. 14). Thus, we suggest that the monazite core and the small low-Ca garnet core (Fig. 4A) likely formed during a period of contact metamorphism related to the granodiorite intrusion. One monazite grain in sample WF-1 is partially included in biotite and two others are entirely included in muscovite; most of the other analyzed grains are matrix grains that are elongate parallel to foliation. Thus, the Devonian age of monazite, 390 ± 4.5 Ma, in this sample is the maximum age of foliation-forming phyllosilicates and may constrain the timing of the main period of metamorphism. Similar, middle to late Devonian monazite ages have been reported in the Wissahickon Formation from the sillimanite zone in Philadelphia (~380 Ma; Bosbyshell, 2008) and in rock along strike from WF-1, approximately 15 km to the southwest (377 ± 6.6; Bosbyshell, 2001). Slightly discordant late Devonian monazite ages were previously obtained using TIMS from both the staurolite and sillimanite zones along Wissahickon Creek (Bosbyshell et al., 1998). Kyanite-grade overprinting in the Wissahickon Formation nearer the Wilmington Complex is also Devonian in age (Bosbyshell, 2001; Pyle et al., 2006).

Monazite in sample WF-2 further constrains the tectonic history in the Wissahickon Formation. The sequence of metamorphism and deformation that can be deduced from textures in WF-2, as described above, is: (1) growth of garnet cores during low pressure metamorphism, (2) deformation to produce the dominant foliation, (3) growth of garnet during higher pressure metamorphism followed by (4) additional deformation, resulting in shear bands and garnet rotation. The lack of curvature of the included fabric in the rotated garnet demonstrates that rotation is post-garnet growth (Fig. 8). The age of monazite cores in WF-2, 431 ± 3 Ma, is essentially the same as the crystallization age of the nearby Springfield Granodiorite (Fig. 1) and is interpreted as the age of the early low-pressure metamorphism. High U-rims on monazite are elongate and, in some cases asymmetric, parallel to foliation and their age, late Silurian to early Devonian, is interpreted as marking the growth of the dominant foliation.

The range of rim ages in WF-2, 425 ± 4 Ma to 404 ± 6 warrants comment. Two of the grains analyzed on the Ultrachron in this study were previously analyzed on the SX-50 microprobe (Bosbyshell, 2001), yielding similar U content and ages, suggesting that the range of rim ages is reproducible and not due to a lack of analytical precision. This leads to an explanation that monazite growth and deformation were episodic in a long-lived geochemical environment that favored the growth of the high-U rims. The presence of monazite with high-U rims as inclusions within high-Ca overgrowth on garnet (Fig. 14) and the observation that the high-Ca garnet overgrowth is younger than the fabric to which the monazite is parallel (Figs. 7D, 8B) requires the higher pressure metamorphism to be younger than the monazite rims. Thus, kyanite-grade metamorphism must be younger than the late Silurian to early Devonian age of monazite rims, consistent with the results for WF-1, above, and with previous results

(Bosbyshell, 2001, 2008; Bosbyshell et al., 1998) which indicate that this period of metamorphism is middle to late Devonian in age.

Orogen-scale comparisons and tectonic interpretations

The age of monazite cores in the Doe Run Schist, ~455 Ma, is similar to well-documented deformation and syn-tectonic deposition in foreland basin rocks of southeastern Pennsylvania (Ganis and Wise, 2008; Wise and Ganis, 2009) and syn-collisional tonalitic and granodioritic magmatism in northern Virginia and Maryland (Sinha et al., 2012) resulting from the Taconic orogeny. Thus, monazite growth and early prograde metamorphism in the Doe Run Schist are interpreted as products of tectonic burial and heating resulting from the Taconic orogeny (Fig. 15). While only one monazite core of this age was analyzed in the Mt. Cuba Gneiss, x-ray composition maps indicate that additional cores with similar bulk composition are present and likely formed at the same time. Thus, this unit was also likely involved in middle Ordovician Taconic orogenesis.

Maximum temperatures in the Mt. Cuba gneiss were attained during the middle Silurian, some 15 to 20 million years after the end of the Taconic orogeny, which is recognized by the cessation of foreland deformation and deposition of the lower Silurian Shawangunk basal conglomerate in the Appalachian basin (Wise and Ganis, 2009). Middle Silurian metamorphism could result from thermal relaxation of the crust following Taconic burial and crustal thickening. However, Silurian-aged magmatism in the central Appalachians of Maryland and Virginia is thought to reflect an extensional regime as a result of either slab delamination or a back-arc setting related to a younger subduction zone (Sinha et al., 2012). Either scenario, thermal relaxation or an extensional setting, would produce an elevated geothermal gradient along the Laurentian margin during the early to middle Silurian which likely contributed to the metamorphic thermal budget.

Our results together with those of Aleinikoff et al. (2006) indicate that maximum temperatures in the Mt. Cuba gneiss within the Mill Creek nappe were attained ca. 425 Ma, prior to the highest temperatures in the structurally lower Avondale nappe which were attained after 415 Ma. In turn, peak metamorphism in the structurally lowest unit, the Doe Run Schist in the West Chester nappe, is even younger – maximum temperatures at this level were not reached until 409 Ma, in the early Devonian. We interpret this sequence to represent successive stacking of thrust sheets from southeast to northwest (present geography) with the warmer overriding sheets contributing to heating of the lower sheets.

This deformation and metamorphism is interpreted to be the result of the Silurian approach and collision of peri-Gondwana terranes, Carolinia and Ganderia (Fig. 16), in a dominantly sinistral transpressive tectonic regime (Hibbard, 2000; Hibbard et al., 2007; 2010). Hibbard et al. (2007) suggest that the New York promontory acted as a restraining bend in this transpressive setting and was the site of intense tectonism at this time. The thrust slices containing the Doe Run Schist and Mt. Cuba gneiss occupy a crustal block that is bounded by steeply dipping shear zones: the Pleasant Grove-Huntingdon Valley zone to the northwest and the Rosemont zone to the southeast; the geometry of the thrust faults relative to the steeply dipping shear zones (Fig. 16A) is consistent with a sinistral restraining bend as proposed by Hibbard et al. (2007). The most recent ductile deformation in these shear zones is thought to reflect dextral motion (Valentino et al., 1994; 1995); such motion could have translated this block to its present location from a position nearer the New York promontory.

The tectonic and metamorphic history of the Wissahickon Formation is markedly different from that of the West Grove Metamorphic Suite (Fig. 15). Silurian-aged metamorphism (430 to 440 Ma; Bosbyshell, 2001; Pyle et al., 2006) is pervasive in the Wissahickon Formation nearest the Wilmington Complex, but elsewhere in the Wissahickon Formation the predominant metamorphism is middle to late Devonian in age (Bosbyshell, 2001; 2008). Bosbyshell et al. (1999) recognized a low pressure facies series gradient in the Wissahickon Formation from cordierite-bearing rocks nearest the granulite-facies Wilmington Complex and Silurian-aged Arden Plutonic Suite (Plank et al., 2000; Aleinikoff et al, 2006) through sillimanite + K-feldspar, sillimanite + muscovite, to andalusite-bearing assemblages over a map distance of approximately 10 km. The results presented here indicate that the grade of the early metamorphism continued to decrease to the east (present coordinates), where rocks of the Wissahickon Formation type section exhibit scant evidence for metamorphism at this time. Garnet cores (Fig. 7A), which likely formed in a contact metamorphic setting adjacent to a small granodiorite body, and monazite cores (as in sample WF-1) which yield a Silurian age, are the only evidence for Silurian metamorphism in the type section of Wissahickon Creek. Bosbyshell (2008) describes evidence for an early period of metamorphism to the south of Wissahickon Creek in Philadelphia, where the rocks are in close proximity to the Silurian-aged (427 ± 3 Ma)

Springfield Granodiorite (Bosbyshell et al., 2005). Thus, it appears that, away from intrusions, the Wissahickon Formation remained at low-metamorphic grade until the Devonian.

The middle Devonian age of monazite suggests that metamorphism in the Wissahickon Formation is the result of crustal thickening during the Acadian orogeny, the accretion of Avalon in the northern Appalachians (Fig. 15). Rocks of known Gondwanan affinity are not exposed in the central Appalachians at the latitude of the study area and, until recently, the effects of the Acadian orogeny in southeastern Pennsylvania were the subject of reasoned inference (Amenta, 1974; Valentino et al., 1995) or were considered to be absent (Faill, 1997). Metamorphism of this age is well known in southern New England (Lanzirotti and Hanson, 1996; Robinson et al., 1998; Lancaster et al., 2008). Given the evidence for younger, dextral transcurrent motion regionally on the Pleasant Grove/Huntington Valley and Rosemont shear zones (Valentino et al., 1994; 1995) and throughout the Appalachians (e.g., Dennis, 2007; Hibbard and Waldron, 2009) we propose that the crustal block east of the Rosemont shear zone, which contains the Wissahickon Formation and Wilmington Complex, was originally located some distance to the north. The block may represent a truncation of the New York promontory, analogous to the relationship of the State Line flexure (of North and South Carolina) to the Virginia promontory in the southern Appalachians as proposed by Hibbard and Waldron (2009).

A reversal from sinistral transpression in the Silurian through middle Devonian to dextral motion in the late Devonian and younger would result in the restraining bend described above (Fig. 16) becoming a releasing bend and in turn facilitate extension, uplift and cooling in the region. This is consistent with the relatively rapid cooling implied by ^{40}Ar-^{39}Ar ages for rocks in the study area. Blackmer et al. (2007) report hornblende ages that indicate cooling of the Avondale nappe through the ~500 °C isotherm at ~400-375 Ma and white mica ages from rock throughout the study area of ~365 Ma indicative of cooling through ~350 °C. Textures consistent with rapid and isothermal decompression are not present in the pelitic rocks analyzed in this study, but such textures have been described in gneiss of the Avondale nappe (Johnson and Bosbyshell, 2010; Trice et al., 2014).

Implications

In-situ analysis of monazite is a powerful tool for dating complexly deformed, polymetamorphic terranes such as the ancient Appalachians. When monazite growth can be linked to reactions between silicate minerals, as in our examples from the West Grove Metamorphic Suite, an age can be assigned to the attainment of specific metamorphic pressure and temperature conditions. However, monazite in polymetamorphic rocks may develop zoning over time scales that cannot be resolved by EPMA. Here, the age of monazite inclusions in metamorphic porphyroblasts, in combination with fabric-porphyroblast relationships can be used to apply timing constraints to the pressure-temperature-deformation history of rocks. Syntectonic monazite growth may directly constrain the timing of foliation development, as in the Wissahickon Formation.

Our application of these methods to one geographically-limited area leads to outcomes with broad implications for the history of the Appalachians and other complex orogens. The New York promontory has been long recognized as the geographic boundary between the northern and southern Appalachians. Hibbard et al. (2010) described this region as the area where first-order contrasts between different segments of the orogen appear. We suggest that this may be a false dichotomy for early Paleozoic tectonism. Our work demonstrates diachronous attainment of peak metamorphic temperatures across a series of nappes in Laurentian margin rock during the late Silurian through early Devonian. This shows that, in contrast with models involving discrete southern (Cherokee) and northern (Salinic) orogenies, the approach and accretion of peri-Gondwanan terranes in a left-lateral transpressive regime spanned the entire orogen.

An additional outcome is the recognition of significant Middle Devonian metamorphism – the effects of the Acadian orogeny – in the central Appalachians. Based on current data (e.g. Hibbard et al., 2010), the Middle Devonian accretion of Avalonia is the most significant northern Appalachian event which has no southern counterpart. One interpretation of our results could be that the central Appalachians, though geographically contiguous with the southern Appalachians, experienced this northern Appalachian tectonism and that the New York promontory should not be considered the fundamental boundary within the orogen. However, we propose that the units which record Acadian (Middle Devonian) metamorphism and deformation (the Wissahickon Formation and Wilmington Complex arc) may correlate with units in the northern Appalachians (Bosbyshell et al., 2015) and likely originated some distance north of their current geographic location. These units were juxtaposed against Laurentian margin rocks (the West Grove Metamorphic Suite) in a right-lateral transcurrent regime. Thus, questions emerge concerning the scale of the transcurrent motion along the plate boundary at this time and the identity and location of other units which may have been juxtaposed.

Modern convergent plate boundaries are similarly complex along strike. Our findings demonstrate the value of detailed deformational and metamorphic histories within relatively small areas in contributing to a more nuanced understanding of orogen-scale accretionary processes and timing.

Acknowledgements

We gratefully acknowledge the contributions of Julian Allaz, Mike Jercinovic and Mike Williams of University of Massachusetts Ultrachron lab and Fred Monson of the Center for Microanalysis Imaging Research and Training at West Chester University. West Chester University students Jason Bukeavich, Emily Caufman, Tracy Ellis, Richard Henson, Chelsie Johnston, Maureen Moore, and Kirk Seagers contributed to our research. This work was funded by the Pennsylvania Geological Survey and the United States Geological Survey through the USGS National Cooperative Geologic Mapping Program and by faculty-development grants from the College and Arts and Sciences of West Chester University. We thank Mike Williams for his constructive comments on an early version of this manuscript. We also thank the two anonymous reviewers whose comments and suggestions greatly improved the final version.

Figure captions.

1. (A) Geologic map of southeastern Pennsylvania and northern Delaware, modified after Blackmer (2005) and Plank et al. (2000). PGHVsz = Pleasant Grove – Huntingdon Valley shear zone. (B) Map of Appalachian orogen after Hibbard et al. (2006), arrow indicates location of map (A).

2. Contoured equal area plots comparing the orientation of poles to foliation in (A) the West Grove Metamorphic Suite (WGMS), (B) the Rosemont Shear Zone (RSZ) and (C) the Wissahickon Formation (WF). Data in (A) are compiled from Blackmer (2004a, 2004b) and Wiswall (2005); data in (B) and (C) are from Bosbyshell (2001). Data are plotted using Stereonet 8 (Allmendinger et al., 2012; Cardozo and Allmendinger, 2013). (D) Schematic cross-section of study area. PGHVsz = Pleasant Grove – Huntingdon Valley shear zone; ET = Embreeville Thrust; SRF = Street Road Fault; MC = base of Mill Creek nappe; OP = Octoraro Phyllite; PCS = Peters Creek Schist.

3. (A) Photomicrograph of sample DR-1. Note occurrence of garnet and sillimanite along embayed edge of staurolite. (B) Sillimanite along edge of staurolite in DR-2. Scale bar in both photomicrographs is 1 mm.

4. (A) X-ray composition maps illustrating zoning in garnet from DR-2. Scale bar is 1 mm. (B and C) Pressure-temperature diagram for DR-2 based on an equilibrium assemblage diagram calculated with THERIAK-DOMINO (de Capitani and Petrakakis, 2010) using database tcdb55c2d (THERMOCALC; Powell and Holland 1994; Powell et al. 1998; White et al., 2007). Dashed arrow shows possible P-T path. (A) Garnet growth in the presence of staurolite, grossular content decreases slightly; (B) amount of garnet in assemblage is constant as staurolite consumes chlorite and chloritoid; (C) at the chlorite-out reaction, garnet is consumed as staurolite grows; until (D) garnet with greater grossular content grows rapidly at the high temperature limit of staurolite stability. Compositional isopleths of garnet rim composition intersect at approximately 550 MPa and 700 °C. The bulk composition used in the calculation is given in Table 2; garnet analysis, Table 3.

5. Photomicrographs from sample MC-1 in the Mt. Cuba Gneiss showing (A) staurolite overgrowing a sillimanite fabric and (B) kyanite overprinting a cluster of fibrolite. (C) X-ray composition maps of typical garnet in MC-1. Scale bar in A = 1 mm; B = 0.5 mm; C = 0.6 mm.

6. Pressure-temperature diagram for MC-1 based on an equilibrium assemblage diagram calculated with THERIAK-DOMINO (de Capitani and Petrakakis, 2010) using database tcdb55c2d (THERMOCALC; Powell and Holland 1994; Powell et al. 1998; White et al., 2007). Shaded area corresponds to stability fields of staurolite-bearing assemblages; isopleths of biotite abundance (moles) and XGrs in garnet are plotted within the field of the maximum temperature mineral assemblage. The bulk composition used in the calculation is given in Table 2; garnet analysis in Table 3. See text for discussion.

7. X-ray composition maps of garnet from the Wissahickon Formation. (A) WF-Sil, sillimanite zone; (B) WF-Ky, staurolite + kyanite zone; (C) WF-1, staurolite zone; (D) WF-2, western kyanite (after andalusite) zone.

8. Photomicrographs of Wissahickon Formation samples. (A) WF-1. The garnet pictured in (A) is shown in X-ray maps in Figure 7. Note small low-Ca core in X-ray map from Figure 7 is visible, surrounded by inclusions. (B) Sample WF-2; garnet at right is shown in X-ray elemental maps in Figure 7D. The inclusion free core is visible; note that inclusion trails in the outer portion of the garnet are parallel to external foliation. The core of the center garnet is not in the plane of the thin section, so foliation-parallel inclusions to pass through the entire grain. Inclusion trails in the garnet at left are at a high angle to foliation.

9. Pressure-temperature diagram for WF-1 based on an equilibrium assemblage diagram calculated with THERIAK-DOMINO (de Capitani and Petrakakis, 2010) using database tcdb55c2d (THERMOCALC; Powell and Holland 1994; Powell et al. 1998; White et al., 2007). The stable assemblage in the field where garnet isopleths intersect is labeled, as are the rutile-in and -out, garnet-in, kyanite-in reaction boundaries. The bulk composition used in the calculation is given in Table 2; garnet analysis, Table 3. Al2SiO5 phase boundaries are shown for reference; the phases are not part of all assemblages except where indicated.

10. Summary of monazite results. Histograms show a Gaussian distribution calculated using the weighted mean and standard distribution of monazite results. Distributions which are labeled and outlined in bold lines are the weighted mean of n compositional domains; curves without the bold highlight are the results of individual compositional domains that are not used in the weighted averages. Results with an asterisk (*) indicate analyses performed at RPI. For sample DR-2, n is the number of individual spot analyses used. In all other samples n is the number of dated domains used in the average age calculation. See text for additional information; see Table 3 for monazite analyses.

11. (A) Backscattered electron (BSE) image of an elongate, asymmetric monazite in sample DR-1; grain shape suggests syntectonic growth. Scale bar = 200 µm. (B) Ca X-ray map of garnet superimposed on BSE image to show location of m1 in low-Ca rim, sample DR-2. Scale bar is 0.5 mm. Analyses from the low-Y rim (circles) yield an early Devonian age, constraining the timing of maximum temperatures in this rock. (C) A monazite inclusion within staurolite, in a microlithon from sample DR-2, lacks the low-Y overgrowth. Scale bar in BSE image is 1 mm.

12. (A) Photomicrograph of garnet in sample MC-1 rimmed with Al2SiO5 (kyanite) with monazite (grain m204) partially included in both garnet and plagioclase. Scale bar = 250 µm. (B) BSE image Al2SiO5 surrounding garnet; morphology is consistent with kyanite. (C) X-ray composition maps of monazite. High-Th rim yields a Devonian age. Width of field is 72 µm. See text for discussion.

13. Rose diagrams showing orientation of the long dimension of monazite grains in oriented thin sections from the location of sample 44069 of Aleinikoff et al. (2006). (A) Orientation of 190 grains in sections oriented perpendicular to strike of foliation; maximum on rose diagram corresponds to 34 grains. White bar is approximate dip of foliation. (B) Orientation of 98 grains in sections cut parallel to strike, maximum corresponds to 15 grains.

14. X-ray composition maps of monazite in the Wissahickon Formation. (A) Monazite grain (m89) from sample WF-1. Small, low-Th, high-Y core yields a Silurian age (428 ± 4 Ma); remainder of grain is Devonian (383 ± 2.5 Ma). Scale bar = 50 μm. (B) Uranium X-ray maps from sample WF-2. Grain m5 is an inclusion in the high-Ca overgrowth on the center garnet in Figure 8. Thus, the early Devonian ages of the high-U rims constrain the maximum age for growth of this garnet. Scale bars in m1 and m2 = 50 μm; in m5 = 30 μm.

15. Summary of geochronologic and metamorphic results compared with proposed southern and northern Appalachian orogenies. Patterned areas indicate deformation; bubble indicates granodioritic magmatism. Timing of Appalachians orogenies from Robinson et al., (1998), Hatcher (2005), Wise and Ganis (2009), and Hibbard et al. (2010). Monazite results for the Mill Creek nappe are from Aleinikoff et al. (2005); an additional Wissahickon Formation data set from Philadelphia (Bosbyshell, 2008) is also plotted. MCG = Mt. Cuba Gneiss; DRS = Doe Run Schist.

16. A. Schematic geologic map illustrating that the geometry of the thrust sheets in relation to the steeply dipping shear zones is consistent with a sinistral transpressive regime. The timing of metamorphism, with peak temperatures attained in the structurally lowest block subsequent to those in higher sheets, is interpreted to be the result of successive stacking of thrust sheets from southeast to northwest with the warmer overriding sheets contributing to the thermal budget of lower sheets. B. Plate tectonic reconstruction for the Silurian modified from Hibbard et al. (2007) illustrating approach of Ganderia in sinistral transpression. Rectangle shows possible location of deformation shown in A. PGHVsz = Pleasant Grove – Huntingdon Valley shear zone; EvT = Embreeville Thrust; SRF = Street Road Fault; MC = unnamed fault below Mill Creek anticline; RSZ = Rosemont shear zone.

References

Alcock, J. (1989) Tectonic units in the Pennsylvania-Delaware Piedmont: Evidence from regional metamorphism and structure. Ph.D. thesis, University of Pennsylvania, Philadelphia, 259 p.

Alcock, J. (1994) The discordant Doe Run thrust—Implications for stratigraphy and structure in the Glenarm Supergroup, southeastern Pennsylvania Piedmont. Geological Society of America Bulletin, 106, 932–941.

Alcock, J. and Wagner, M.E. (1995) Metamorphic discontinuities in the Pennsylvania – Delaware Piedmont: evidence for early Paleozoic assembly. Canadian Journal of Earth Science, 32, 686-698.

Aleinikoff, J.L, Schenck, W. S., Plank, M. O., Srogi, L. A., Fanning, C. M., Kamo, S. L., and Bosbyshell, H. (2006) Deciphering igneous and metamorphic events in high-grade rocks of the Wilmington Complex, Delaware: Morphology, cathodoluminescence and backscattered electron zoning, and SHRIMP U-Pb geochronology of zircon and monazite. Geological Society of America Bulletin, 118, 39-64.

Allmendinger, R. W., Cardozo, N. C., and Fisher, D. (2012) Structural Geology Algorithms: Vectors &Tensors: Cambridge, England, Cambridge University Press, 289 pp.

Amenta, R. V. (1974) Multiple deformation and metamorphism from structural analysis in the eastern Pennsylvania Piedmont: Geological Society of America Bulletin, 85, 1647-1660.

Bascom, F., Clark, B., Darton, N.H., Kummel, H.B., Salisbury, R.D., Miller, B.L., and Knapp, G.N. (1909) Philadelphia folio, United States Geological Survey Geological Atlas of the U.S., Folio 162.

Bascom, F., and Stose, G. W. (1932) Description of the Coatesville and West Chester quadrangles, United States Geological Survey Atlas of the U.S., Folio 223.

Bascom, F., and Stose, G.W. (1938) Geology and mineral resources of the Honeybrook and Phoenixville Quadrangles. United States Geological Survey Bulletin, 891 1-145.

Blackmer, G.C. (2004a) Bedrock geology of the Coatesville quadrangle, Chester County, Pennsylvania. Pennsylvania Geological Survey, 4th ser., Atlas 189b, CD-ROM.

Blackmer, G. C. (2004b) Bedrock geologic map of the Pennsylvania portion of the Kennett Square quadrangle, Chester County, Pennsylvania. Pennsylvania Geological Survey, 4th ser., Open-File Report OFBM 04–01.0, 14 p., Portable Document Format (PDF).

Blackmer, G.C. (2004c) Speculation on the tectonic history of the Glenarm Group and associated parts of the Wissahickon Formation, in Blackmer, G.C., and Srogi, L., Marginalia –

Magmatic arcs and continental margins in Delaware and southeastern Pennsylvania: Guidebook, 69th Annual field Conference of Pennsylvania Geologists, West Chester, PA, 15-27.

Blackmer, G.C. (2005) Preliminary bedrock geologic map of a portion of the Wilmington 30- by 60-minute quadrangle, southeastern Pennsylvania. Pennsylvania Geological Survey, 4th ser., Open-File Report OFBM 05–01.0, 16 p., Portable Document Format (PDF).

Blackmer, G. C. and Bosbyshell H. (2002) The Wissahickon Formation: A persistent problem in the Central Appalachian Piedmont: Geological Society of America Abstracts with Programs, 34, 77.

Blackmer, G.C., Kunk, M.J., Southworth, S., and Bosbyshell, H. (2007) Timing of metamorphism and deformation in southeastern Pennsylvania and northern Delaware: Geological Society of America Abstracts with Programs, 39, n. 1, 75.

Blackmer, G.C., Bosbyshell, H., and Shank, S. (2010) Bedrock geologic map of the Kirkwood quadrangle and Pennsylvania portion of the Rising Sun quadrangle, Chester and Lancaster Counties, Pennsylvania. Pennsylvania Geological Survey, 4th ser., Open-File Report OFBM 10–02.0, 29 p., Portable Document Format (PDF).

Bliss, E.F., and Jonas, A.I. (1916) Relation of the Wissahickon mica gneiss to the Shenandoah limestone and the Octoraro schist of the Doe Run and Avondale region, Chester County, Pennsylvania. U.S. Geological Survey Professional Paper 98, 9–34.

Bosbyshell, H. (2001) Thermal evolution of a convergent orogen: Pressure–Temperature–Deformation–Time paths in the central Appalachian Piedmont of Pennsylvania and Delaware [Ph.D. thesis]: Bryn Mawr, Pa., Bryn Mawr College, 233 p.

Bosbyshell, H. (2005a) Bedrock geologic map of the Lansdowne and Pennsylvania portion of the Bridgeport quadrangles, Delaware, Montgomery, and Philadelphia counties, Pennsylvania. Pennsylvania Bureau of Topographic and Geologic Survey, Open-file Report OFBM-05-05.0, 1 sheet.

Bosbyshell, H. (2005b) Bedrock geologic map of the Pennsylvania portion of the Marcus Hook quadrangle, Delaware County, Pennsylvania. Pennsylvania Bureau of Topographic and Geologic Survey, Open-file Report OFBM-05-06.0, 1 sheet.

Bosbyshell, H. (2008) Bedrock geologic map of a portion of the Philadelphia quadrangle, Montgomery and Philadelphia Counties, Pennsylvania: Pennsylvania Geological Survey, 4th ser., Open-File Report OFBM 08–05.0, 21 p., Portable Document Format (PDF).

Bosbyshell, H; Sinha, A. K., Crawford, M. L., Fleming, P., Srogi, L., and Lutz, T. M. (1998) Thermal evolution of a convergent orogen; new U/ Pb ages of monazite and zircon from the

Central Appalachian Piedmont: Geological Society of America Abstracts with Programs, 30, 125.

Bosbyshell, H., Crawford, M. L., and Srogi, L. (1999) The distribution of overprinting metamorphic mineral assemblages in the Wissahickon Group, southeastern Pennsylvania, in Gates, A. E., and Valentino, D. W., eds., The Mid-Atlantic Piedmont—tectonic missing link of the Appalachians: Geological Society of America Special Paper 330, 41–58.

Bosbyshell, H., Aleinikoff, J. A., and Blackmer, G. C. (2005) A Silurian age for the Springfield Granodiorite: Tectonic and metamorphic implications for the Central Appalachian Piedmont: Geological Society of America Abstracts with Programs, 37 65.

Bosbyshell, H., Wiswall, C.G., and Blackmer, G.C. (2006) The Embreeville Thrust and Street Road Fault: Convergent tectonics in the Central Appalachian Piedmont, SE Pennsylvania. Geological Society of America Abstracts with Programs, 38, n. 2, 87.

Bosbyshell, H., Blackmer, G.C., Mathur, R., Srogi, L., and Schenck, W.S. (2013) Significance of detrital zircon ages in the central Appalachian piedmont of southeastern Pennsylvania and Northern Delaware: Geological Society of America Abstracts with Programs, 45, 7, 810.

Bosbyshell, H., Blackmer, G.C., Schenck, W.S., and Srogi, L. (2014) Defining the West Grove Metamorphic Suite: Implications for tectonic interpretations of the central Appalachian piedmont, *in*, de Wet, A.P., ed., Field Trip Guide Northeastern Section of the Geological Society of America: Geological Society of America Field Guide, 17-33.

Bukeavich, J.R., Srogi, L., and Blackmer, G.C. (2006) Metamorphism and deformation of the Glenarm Wissahickon in SE Pennsylvania Piedmont: Geological Society of America Abstracts with Programs, 38, 2, 24.

Cardozo, N., and Allmendinger, R. W. (2013) Spherical projections with OSXStereonet: Computers & Geosciences, 51, 0, 193 - 205, doi: 10.1016/j.cageo.2012.07.021.

Crawford, M.L. (1974) Calcium zoning in almandine; a model based on plagioclase equilibria, *in* MacKenzie, W.S. and Zussman, J., eds., The Feldspars: Manchester University Press, 629-644.

Crawford, M. L. (1977) Calcium zoning in almandine garnet, Wissahickon formation, Philadelphia, Pennsylvania: Canadian Mineralogist, 15, 243-249.

Crawford, M.L. (1987) The Wissahickon Schist type section, Wissahickon Creek, Philadelphia, Pennsylvania, *in* Roy, D.C., ed, Northeastern Section of the Geological Society of America Centennial Field Guide Volume 5, 77-80.

Crawford, M. L., and Crawford, W. A. (1980) Metamorphic and tectonic history of the Pennsylvania Piedmont: Journal of the Geological Society of London, 137, 311-320.

Crawford, M. L., and Mark, L. E. (1982) Evidence from metamorphic rocks for overthrusting. Pennsylvania Piedmont, U. S. A. Canadian Mineralogist, 20, 333-347.

Crawford, W.A., and Hoersch, A.L. (1984) The geology of the Honey Brook Upland, southeastern Pennsylvania, *in* Bartholomew, M.J., ed., The Grenville Event in the Appalachians and Related Topics: Geological Society of America Special Paper, 194, 111-125.

de Capitani C. and Petrakakis K. (2010) The computation of equilibrium assemblage diagrams with Theriak/Domino software. American Mineralogist 95, 1006-1016.

Dennis, A.J. (2007) Cat Square basin, Catskill clastic wedge: Silurian-Devonian orogenic events in the central Appalachians and the crystalline southern Appalachians, in Sears, J.W., Harms, T.A., and Evenchick, C.A., eds., Whence the Mountains? Inquiries into the Evolution of Orogenic Systems: A Volume in Honor of Raymond A. Price: Geological Society of America Special Paper 433, 313–329, doi: 10.1130/2007.2433(15).

Dumond, G., McLean, N., Williams, M.L., Jercinovic, M.J., and Bowring, S.A. (2008) High-resolution dating of granite petrogenesis and deformation in a lower crustal shear zone: Athabasca granulite terrane, western Canadian Shield: Chemical Geology, 254, 175-196.

Evans, T.P. (2004) A method for calculating effective bulk composition modification due to crystal fractionation in garnet-bearing schist: implications for isopleth thermobarometry: Journal of Metamorphic Geology, 22, 547-557.

Faill, R.T. and MacLachlan, D.B. (1989) Tectonic terranes of southeastern Pennsylvania: Geological Society of America Abstracts with Programs, 21, 13.

Faill, R.T. and Wiswall, C.G. (1994) The Cream Valley fault: Transform from thrust to strike-slip displacement, *in,* Faill, R.T. and Sevon, W.D., eds., Various aspects of Piedmont geology in Lancaster and Chester counties, Pennsylvania: Harrisburg, Pennsylvania, Guidebook for the 59th Annual Field Conference of Pennsylvania Geologists.

Faill, R. T. (1997) A Geologic history of the North-Central Appalachians. Part 1. Orogenesis from the Mesoproterozoic through the Taconic orogeny: American Journal of Science, 297, 551-619.

Ganis, R.G. and Wise, D.U. (2008) Taconic events in Pennsylvania: Datable phases of a ~20 M.Y. orogeny: American Journal of Science, 29, 167-183, DOI 10.2475/02.2008.03.

Gates, A. E., and Valentino, D. W. (1999) The Mid-Atlantic Piedmont—tectonic missing link of the Appalachians: Geological Society of America Special Paper 330, 41–58.

Gordon, S. G. (1922) Mineralogy of Pennsylvania: Philadelphia Academy of Natural Science Special Publication 1.

Grauert, B., Crawford, M. L., and Wagner, M. E. (1973) U-Pb isotopic analysis of zircons from granulite and amphibolite facies rocks of the West Chester prong and the Avondale anticline, southeastern Pennsylvania: Carnegie Institution of Washington Yearbook, 72, 290-293.

Grauert, B., Wagner, M. E., and Crawford, M. L. (1974) Age and origin of amphibolite-facies rocks of the Avondale anticline (southeastern Pennsylvania) as derived from U-Pb isotopic studies on zircon: Yearbook of the Carnegie Institute of Washington, 73, 1000-1003.

Hatcher, R.D., Jr. (2005) Southern and Central Appalachians, in Selley, R.C., Cocks, L.R.M., and Plimer, I.R., eds., Encyclopedia of Geology: Amsterdam, Netherlands, Elsevier Academic Press, p. 72–81.

Hatcher, R.D., Jr., Bream, B.R., and Merschat, A.J. (2007) Tectonic map of the southern and central Appalachians: A tale of three orogens and a complete Wilson cycle, in Hatcher, R.D., Jr., Carlson, M.P., McBride, J.H., and Martínez Catalán, J.R., eds., 4-D Framework of Continental Crust. Geological Society of America Memoir 200, 595-632.

Hess, D. F. (1981) Further data on andalusite and kyanite pseudomorphs after andalusite from Delaware County, Pennsylvania: Friends of Mineralogy, Pennsylvania Chapter, Newsletter, 9, 3-4.

Heyl, A. V. (1980) Pennsylvania News from Colorado: Friends of Mineralogy, Pennsylvania Chapter, Newsletter, 8, 4-5.

Hibbard, J.P. (2000) Docking Carolina: Mid-Paleozoic accretion in the southern Appalachians: Geology, 28, 127-130.

Hibbard, J.P., van Staal, C.R., Rankin, D.W., and Williams, H. (2006) Lithotectonic map of the Appalachian orogen, Canada–United States of America. Geological Survey of Canada Map 2096A, scale 1:1,500,000.

Hibbard, J.P., van Staal, C.R., and Miller, B.V. (2007) Links among Carolinia, Avalonia, and Ganderia in the Appalachian peri-Gondwanan realm, in Sears, J.W., Harms, T.A., and Evenchick, C.A., eds., Whence the Mountains? Inquiries into the Evolution of Orogenic Systems: A Volume in Honor of Raymond A. Price: Geological Society of America Special Paper 433, 291–311, doi: 10.1130/2007.2433(14).

Hibbard, J.P., van Staal, C.R., and Rankin, D.W. (2010) Comparative analysis of the geological evolution of the northern and southern Appalachian orogen: Late Ordovician–Permian, in Tollo, R.P., Bartholomew, M.J., Hibbard, J.P., and Karabinos, P.M., eds., From Rodinia to Pangea: The Lithotectonic Record of the Appalachian Region: Geological Society of America Memoir 206, 51–69, doi: 10.1130/2010.1206(03).

Hibbard, J.P. and Waldron, J.W.F. (2009) Truncation and translation of Appalachian promontories: Mid-Paleozoic strike-slip tectonics and basin initiation: Geology, 37, 487–490, doi: 10.1130/G25614A.1.

Jercinovic, M.J., Williams, M.L., and Lane, E.D. (2008) In-situ trace element analysis of monazite and other fine-grained accessory minerals by EPMA: Chemical Geology, 254, 197-215.

Knopf, E.B., and Jonas, A.I. (1923) Stratigraphy of the crystalline schists of Pennsylvania and Maryland. American Journal of Science, 5, 40–62.

Lancaster, P.J., Baxter, E.F., Ague, J.J., Breeding, C.M., and Owens, T.L. (2008) Synchronous peak Barrovian metamorphism driven by syn-orogenic magmatism and fluid flow in southern Connecticut, USA: Journal of Metamorphic Geology, 26, 527-538.

Lanzirotti, A. and Hanson, G.M. (1996) Geochronology and geochemistry of multiple generations of monazite from the Wepawaug Schist, Connecticut, USA; implications for monazite stability in metamorphic rocks: Contributions to Mineralogy and Petrology, 125, 332-340.

Mackin, H. (1962) Structure of the Glenarm Series in Chester County, Pennsylvania: Geological Society of America Bulletin, 73, 403-410.

McKinstry, H. (1961) Structure of the Glenarm Series in Chester County, Pennsylvania: Geological Society of America Bulletin, 72, 557-578.

Moore, M.N., Srogi, L., Bosbyshell, H. and Blackmer, G.C. (2007) Retrograde metamorphism of the Glenarm Wissahickon in southeast Pennsylvania: Geological Society of America Abstracts with Programs, 39, n. 6, 319.

Plank, M.O. (1989) Metamorphism in the Wissahickon Formation of Delaware and adjacent areas of Maryland and Pennsylvania [M. A. thesis]: Newark, University of Delaware, 126 p.

Plank, M.O., Schenck, W.S., and Srogi, L. (2000) Bedrock Geology of the Piedmont of Delaware and adjacent Pennsylvania. Report of Investigations No. 59, Delaware Geological Survey, University of Delaware, Newark Delaware, 52 p.

Plank, M.O., Schenck, W.S., Srogi, L., and Plank, T.A. (2001) Geochemistry of the mafic rocks, Delaware Piedmont and adjacent Pennsylvania and Maryland: Confirmation of arc affinity: Delaware Geological Survey Report of Investigations No. 60, 39 p.

Powell, R. and Holland, T.J.B. (1994) Optimal geothermometry and geobarometry: American Mineralogist, 79, 120–133.

Powell, R., Holland, T.J.B., and Worley, B. (1998) Calculating phase diagrams involving solid solutions via nonlinear equations, with examples using THERMOCALC: Journal of Metamorphic Geology, 16, 577–588.

Pyle, J.M. (2006) Temperature–time paths from phosphate accessory phase paragenesis in the Honey Brook Upland and associated cover sequence, SE Pennsylvania, USA. Lithos, 88, 201-232.

Pyle, J.M., Spear, F.S., Rudnick, R.L., and McDonough, W.F. (2001) Monazite–Xenotime–Garnet Equilibrium and a New Monazite–Garnet Thermometer: Journal of Petrology, 42, 2083-2107.

Pyle, J.M., Spear, F.S., Wark, D.A., Daniel, C.G., and Storm, L.C. (2005) Contributions to precision and accuracy of monazite microprobe ages: American Mineralogist, 90, 547-577.

Pyle, J.M., Bosbyshell, H., and Blackmer, G.C. (2006) Refining the metamorphic and tectonic history of the southeastern Pennsylvania Piedmont: Recent results from monazite and zircon geochronology and accessory-phase thermometry, *in* Pazzaglia, F.J., ed., Excursions in Geology and History: Field Trips in the Middle Atlantic States: Geological Society of America Field Guide 8, 83-112.

Robinson, P., Tucker, R. D., Bradley, D., Berry, H. N., Jr., and Osberg, P. H. (1998) Paleozoic orogens in New England, USA: GFF, 120, 119-148.

Schenck, W. S., Plank, M. O., and Srogi, L. (2000) Bedrock geologic map of the Piedmont of Delaware and adjacent Pennsylvania: Delaware Geological Survey, Geologic Map Series No. 10, Scale 1:36,000.

Sinha, A.K., Thomas, W.A., Hatcher, R.D., Jr., and Harrison, T.M. (2012) Geodynamic evolution of the central Appalachian Orogen: Geochronology and compositional diversity of the magmatism from Ordovician through Devonian: American Journal of Science, 275, 481–511.

Spear, F.S., Cheney, J.T., Pyle, J.M., Harrison, T.M., and Layne, G. (2008) Monazite geochronology in central New England: evidence for a fundamental terrane boundary: Journal of Metamorphic Geology, 26, 317–329.

Spear, F.S. and Pyle, J. (2010) Theoretical modeling of monazite growth in a low-Ca metapelite: Chemical Geology, 273, 111-119.

Smith, R. C., and Barnes, J. H. (1994) Geochemistry and geology of metabasalt in southeastern Pennsylvania and adjacent Maryland, *in* Faill, R. T., and Sevon, W. D., eds., Various aspects of Piedmont geology in Lancaster and Chester counties, Pennsylvania: Harrisburg, Pennsylvania, Guidebook for the 59th Annual Field Conference of Pennsylvania Geologists, 45-72.

Smith, R.C., and Barnes, J.H. (2004) White Clay Creek Amphibolite: a Piedmont analog of the Catoctin Metabasalt, in Blackmer, G.C. and Srogi, L., eds., Marginalia – Magmatic arcs and continental margins in Delaware and southeastern Pennsylvania: Guidebook, 69th Annual Field Conference of Pennsylvania Geologists, West Chester, PA., 28-45.

Sutter, J. F., Crawford, M. L., and Crawford, W. A. (1980) 40Ar/39Ar age spectra of coexisting hornblende and biotite from the Piedmont of SE Pennsylvania. Their bearing on the metamorphic and tectonic history. Geological society of America Abstracts with Programs, 12, 85.

Tearpock, D. J., and Bischke, R. (1980) The structural analysis of the Wissahickon schist near Philadelphia, Pennsylvania: Summary: Geological Society of America Bulletin, Part I, 91, 644-647.

Tinkham, D.K. and Ghent, E.D. (2005) Estimating P-T conditions of garnet growth with isochemical phase-diagram sections and the problem of effective bulk-composition: The Canadian Mineralogist, 43, 35-50.

Valentino, D.W., Gates, A.E., and Glover, L., III (1994) Late Paleozoic transcurrent tectonic assembly of the central Appalachian Piedmont. Tectonics, 13, 110-126.

Valentino, D. W., Valentino, R. W., and Hill, M. L. (1995) Paleozoic transcurrent conjugate shear zones in the Central Appalachian Piedmont of southeastern Pennsylvania. Journal of Geodynamics, 19, 303-324.

Valentino, D.W. and Gates, A.E. (2001) Asynchronous extensional collapse of a transpressional orogen: the Alleghanian central Appalachian Piedmont, USA: Journal of Geodynamics, 31, 145–167.

Wagner, M. E., and Srogi, L. (1987) Early Paleozoic metamorphism at two crustal levels and a tectonic model for the Pennsylvania - Delaware Piedmont. Geological Society of America Bulletin, 99, 113-126.

White, R.W., Powell, R., and Holland, J.B. (2007) Progress relating to calculation of partial melting equilibria for metapelites: Journal of Metamorphic Geology, 25, 511-527.

Williams, M. L., Jercinovic, M. J., Goncalves, P., and Mahan, K. (2006) Format and philosophy for collecting, compiling, and reporting microprobe monazite ages: Chemical Geology, 225, 1–15.

Wise, D.U. (1970) Multiple deformation, geosynclinal transitions, and the Martic problem in Pennsylvania, in Fisher, G.W., Pettijohn, F.J., Reed, J.C., and Weaver, K.N., eds., Studies of Appalachian Geology: central and southern. New York, Interscience Publishers, 317-333.

Wise, D.U. and Ganis, R.G. (2009) Taconic Orogeny in Pennsylvania: A ~ 15 – 20 m.y. Apennine-style Ordovician event viewed from its Martic hinterland: Journal of Structural Geology, 31, 887-899.

Wiswall, C.G. (1990) Tectonic history of a terrane boundary based on structural analysis in the Pennsylvania Piedmont. Northeastern Geology, 12, 73-81.

Wiswall, C.G. (2005) Bedrock geologic map of the Unionville quadrangle, Chester County, Pennsylvania. Pennsylvania Geological Survey, 4th ser., Open-File Report OFBM 05–03.0, 15 p., Portable Document Format (PDF).

Wyckoff, D. (1952) Metamorphic facies in the Wissahickon Schist near Philadelphia, Pennsylvania: Geological Society of America Bulletin, 63, 25 - 58.

Table 1. Sample locations

Sample no.	Original no.	Latitude	Longitude	Unit
Monazite geochronology samples				
DR-1	C-207	39.88669°	-75.83834°	Doe Run Schist (WGMS)
DR-2	WG-216	39.83771°	-75.81639°	Doe Run Schist (WGMS)
DR-3	U-05-154	39.91803°	-75.73641°	Doe Run Schist (WGMS)
MC-1	WG-43	39.81778°	-75.79248°	Mt. Cuba Gneiss (WGMS)
MC-2	KS-144	39.85546°	-75.63368°	Mt. Cuba Gneiss (WGMS)
MC-3	44069	39.80792°	-75.67188°	Mt. Cuba Gneiss (WGMS)
WF-1	Ge-06-33	40.08132°	-75.22840°	Wissahickon Formation
WF-2	B-22	39.89227°	-75.35737°	Wissahickon Formation
Other samples				
WF-Ky	Ge-06-09	40.05763°	-75.21914°	Wissahickon Formation
WF-Sil	Ge-06-14	40.02446°	-75.19729°	Wissahickon Formation

TABLE 2. Bulk rock analyses

	DR-2	MC-1	WF-1
SiO_2	54.21	57.14	69.01
TiO_2	2.05	1.23	0.71
Al_2O_3	20.38	20.88	16.38
FeO	6.53	5.61	5.28
Fe_2O_3	5.91	4.80	–
MgO	2.24	2.39	2.16
MnO	0.14	0.23	0.06
CaO	1.52	1.36	0.37
Na_2O	1.21	1.60	1.76
K_2O	2.98	1.90	4.27
LOI	2.44	1.94	
	99.60	99.08	100.00

Note: Samples DR-2 and MC-1 were determined by XRF, WF-1 by EDS. See text for details.

TABLE 3. Garnet Analyses

	DR-1	MC-1	WF-1
FeO	35.93	30.35	29.70
MgO	2.9	3.59	2.53
MnO	1.35	3.92	7.15
CaO	1.91	1.64	2.39
TiO2	0.01	–	–
Al2O3	21.42	20.64	19.87
SiO2	37.2	39.86	38.35
Total	100.72	100.00	100.00
normalized to 12 oxygens			
Fe	2.41	2.00	2.00
Mg	0.35	0.42	0.30
Mn	0.09	0.26	0.49
Ca	0.16	0.14	0.21
Ti	0.00	–	–
Al	2.02	1.92	1.89
Si	2.98	3.15	3.09
alm	0.80	0.71	0.67
sps	0.03	0.09	0.16
grs	0.05	0.05	0.07
pyr	0.12	0.15	0.10

Bosbyshell et al. Figure 1

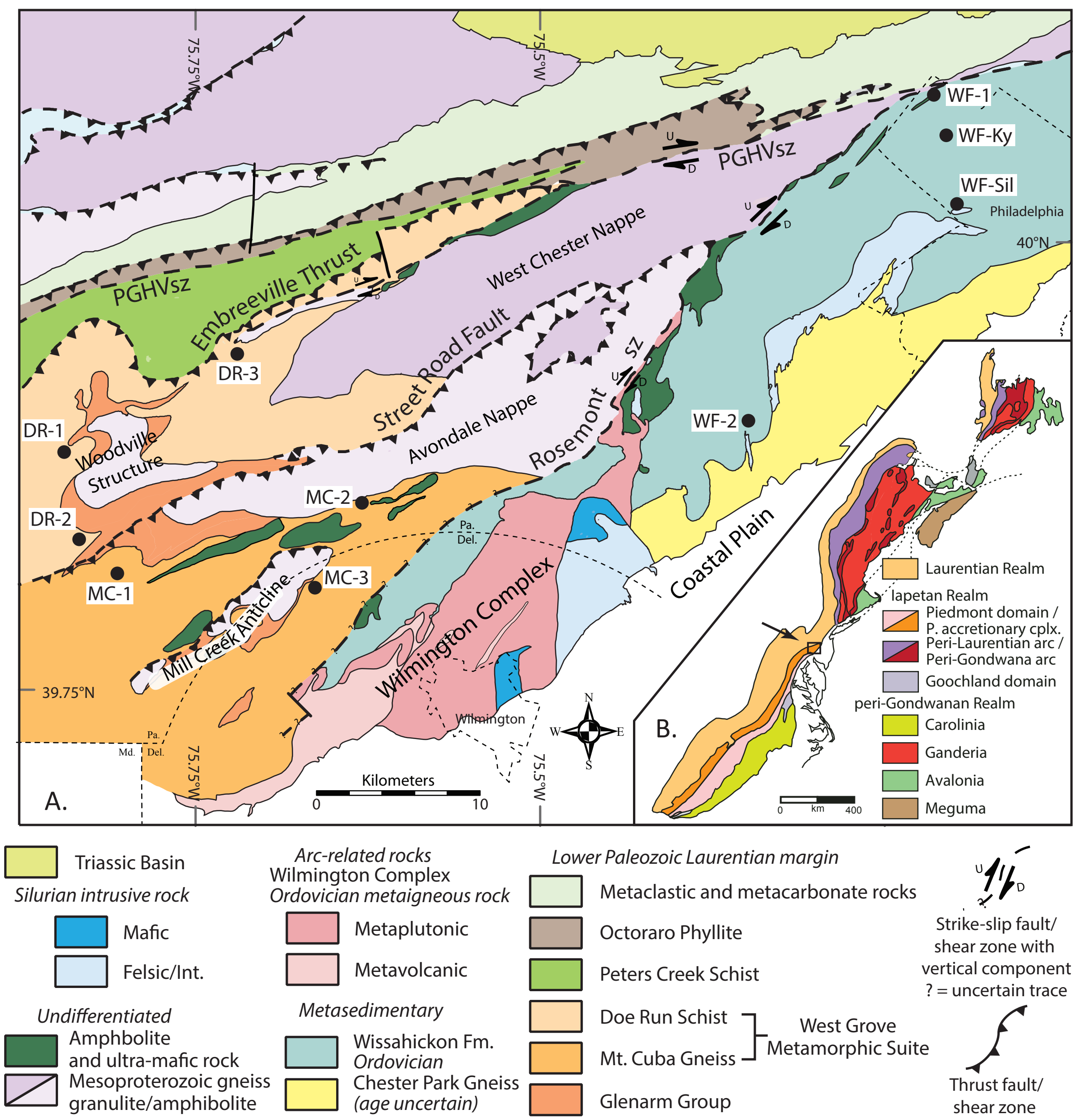

This is a preprint, the final version is subject to change, of the American Mineralogist (MSA)
Cite as Authors (Year) Title. American Mineralogist, in press.
(DOI will not work until issue is live.) DOI: http://dx.doi.org/10.2138/am-2016-5482

Bosbyshell et al. Figure 2

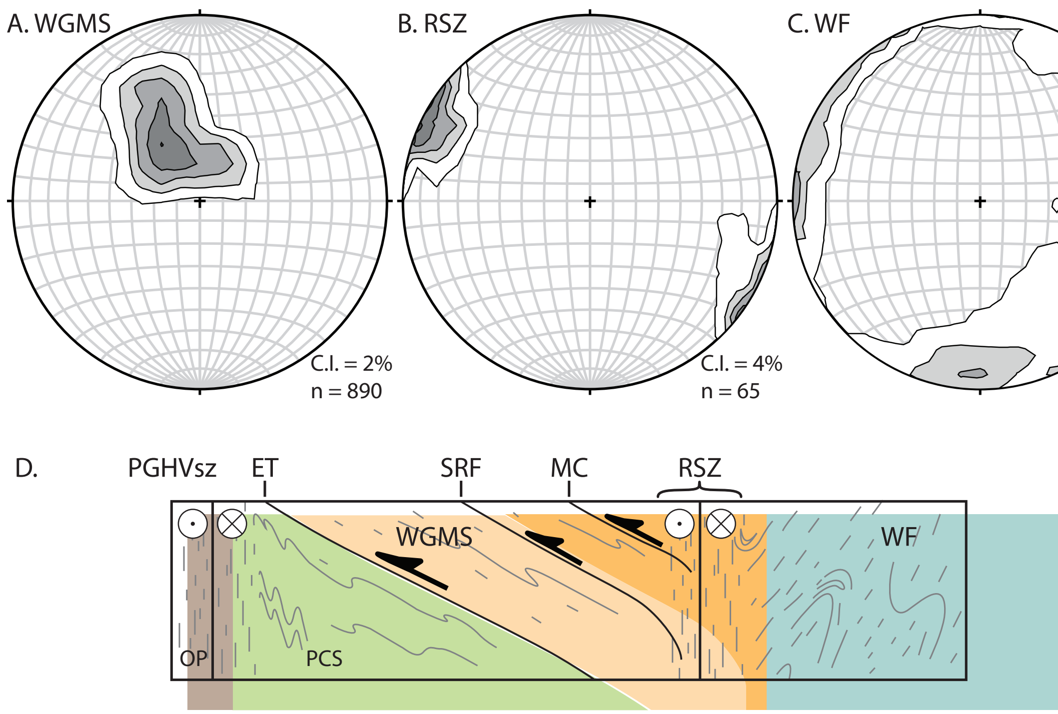

Bosbyshell et al. Figure 3

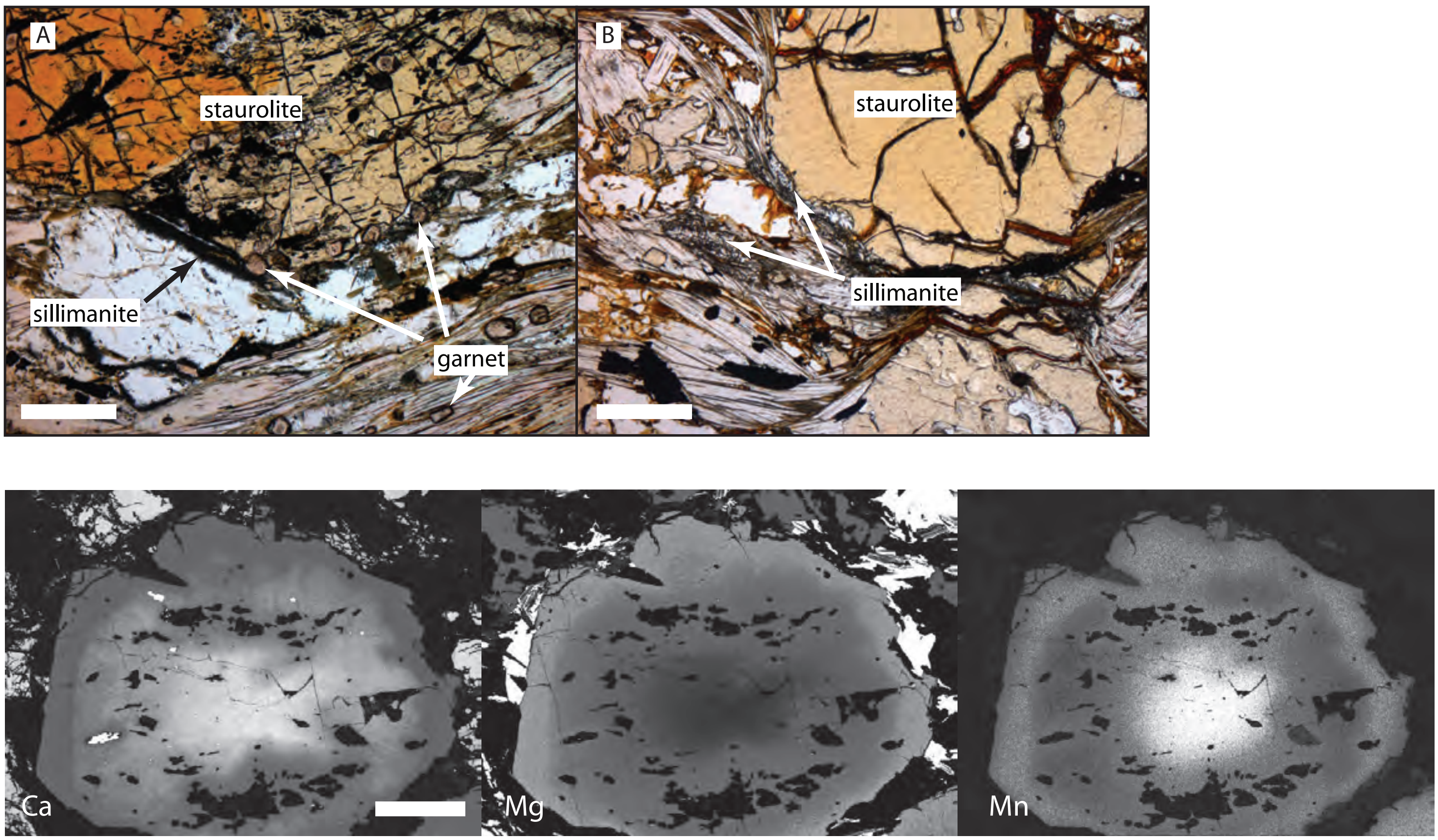

Bosbyshell et al. Figure 4

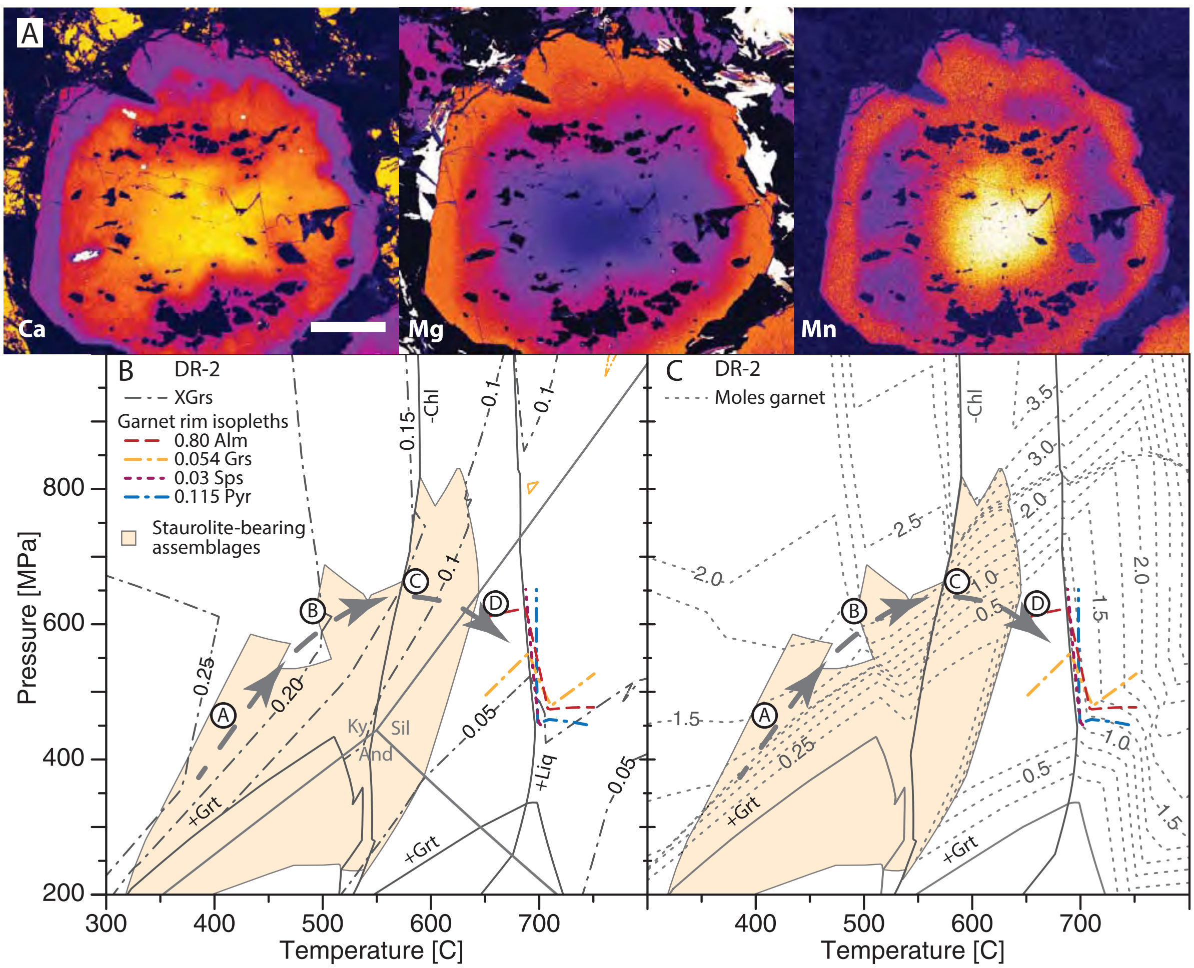

Bosbyshell et al. Figure

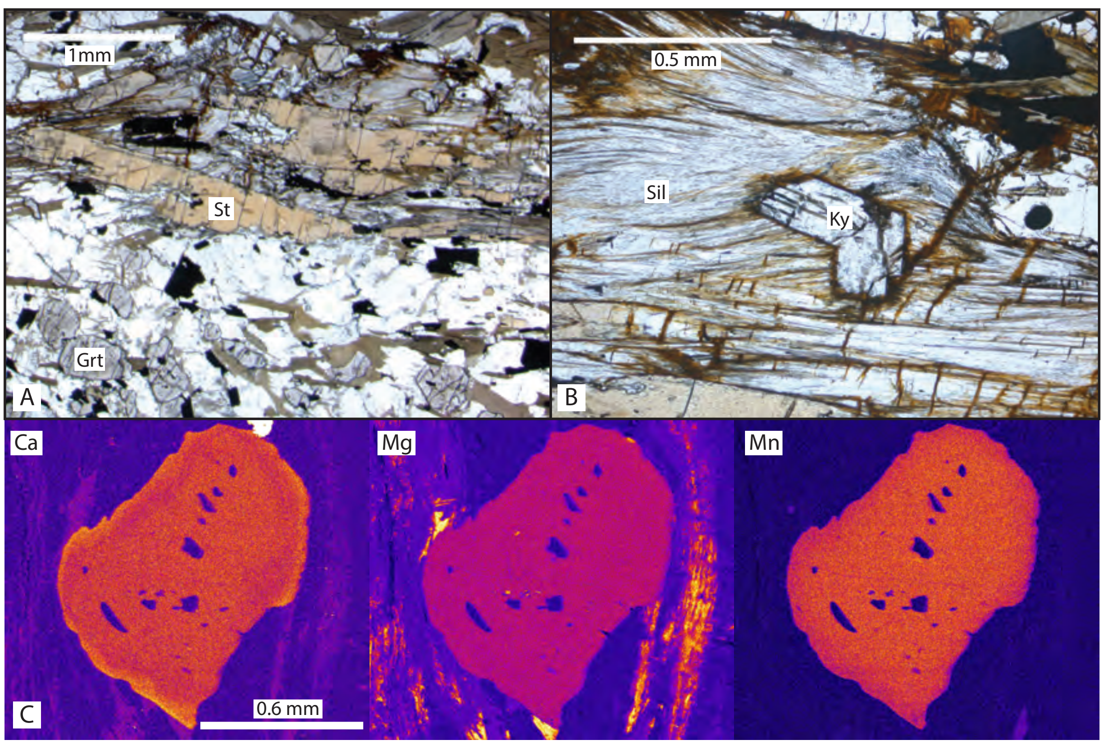

This is a preprint, the final version is subject to change, of the American Mineralogist (MSA)
Cite as Authors (Year) Title. American Mineralogist, in press.
(DOI will not work until issue is live.) DOI: http://dx.doi.org/10.2138/am-2016-5482

Bosbyshell et al. Figure 6

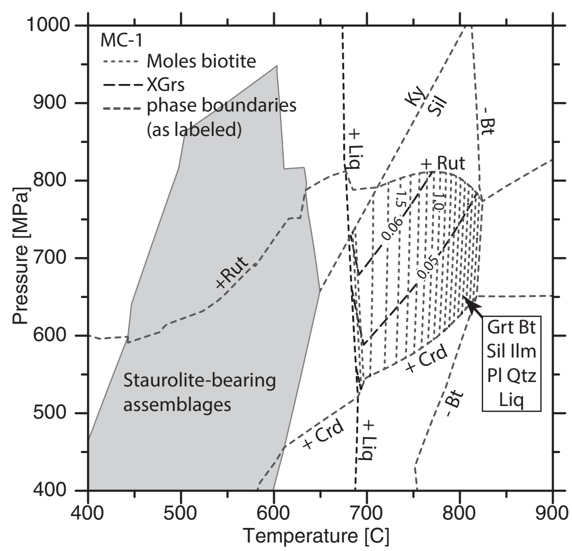

Bosbyshell et al. Figure 7

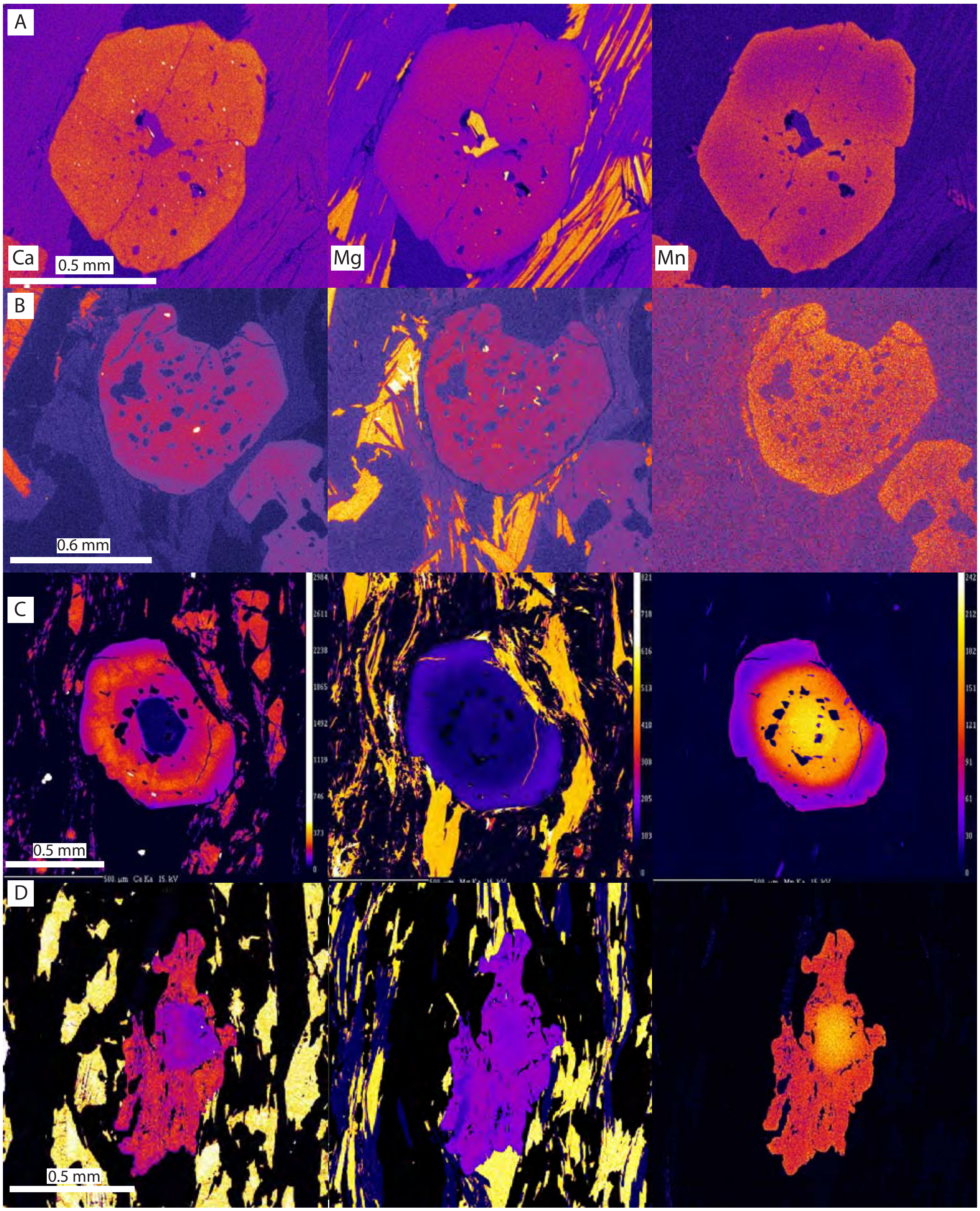

This is a preprint, the final version is subject to change, of the American Mineralogist (MSA)
Cite as Authors (Year) Title. American Mineralogist, in press.
(DOI will not work until issue is live.) DOI: http://dx.doi.org/10.2138/am-2016-5482

Bosbyshell et al. Figure 8

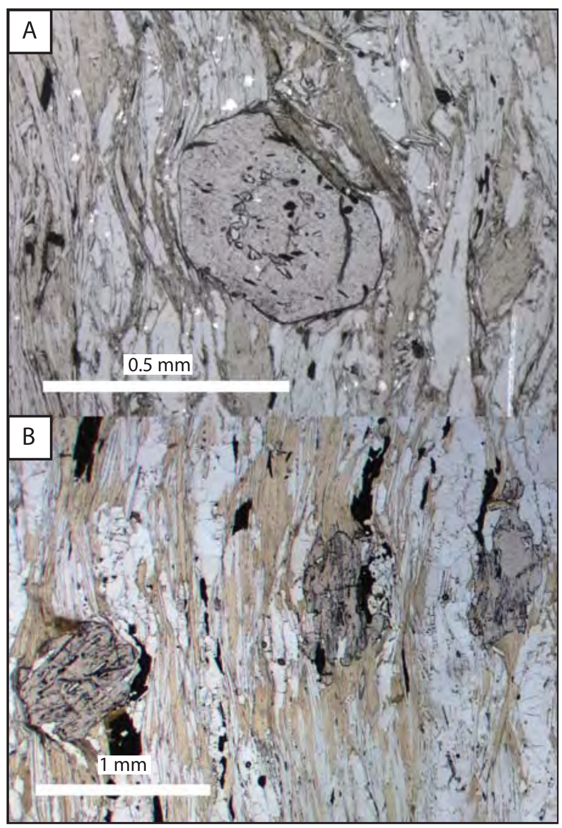

Bosbyshell et al. Figure 9

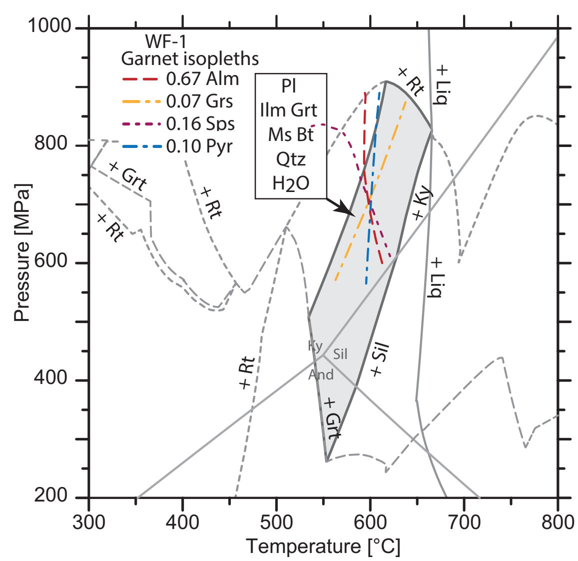

Bosbyshell et al. Figure 10

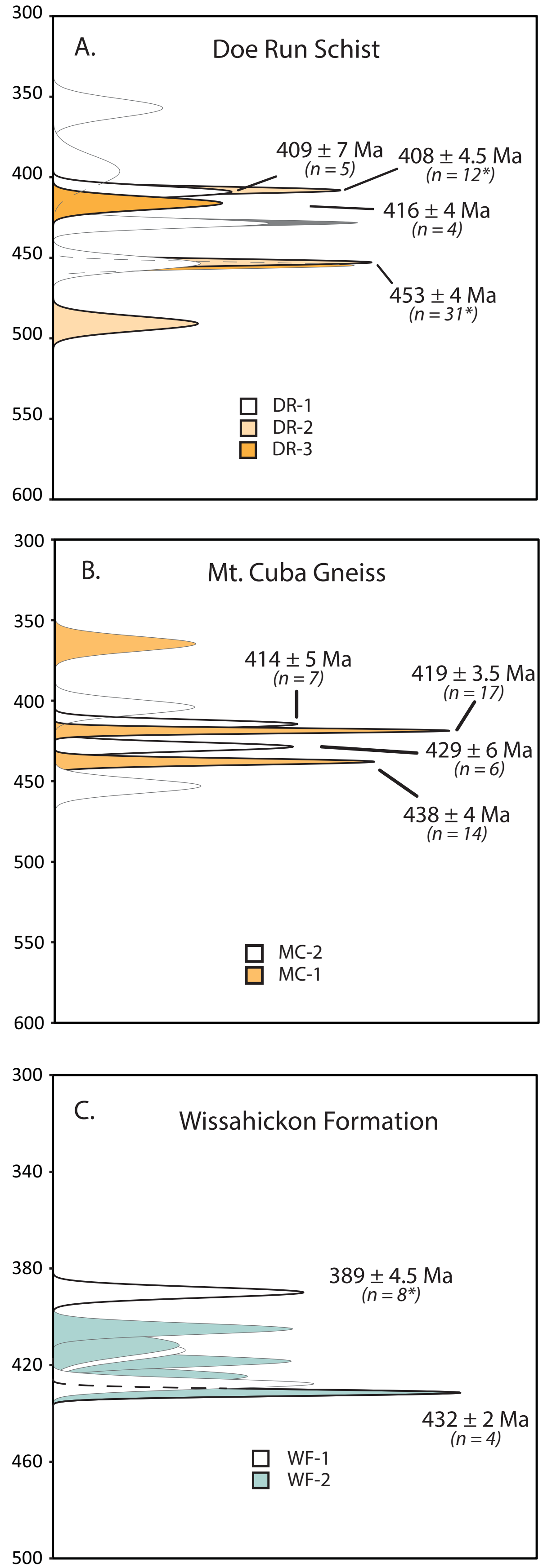

Bosbyshell et al. Figure 11

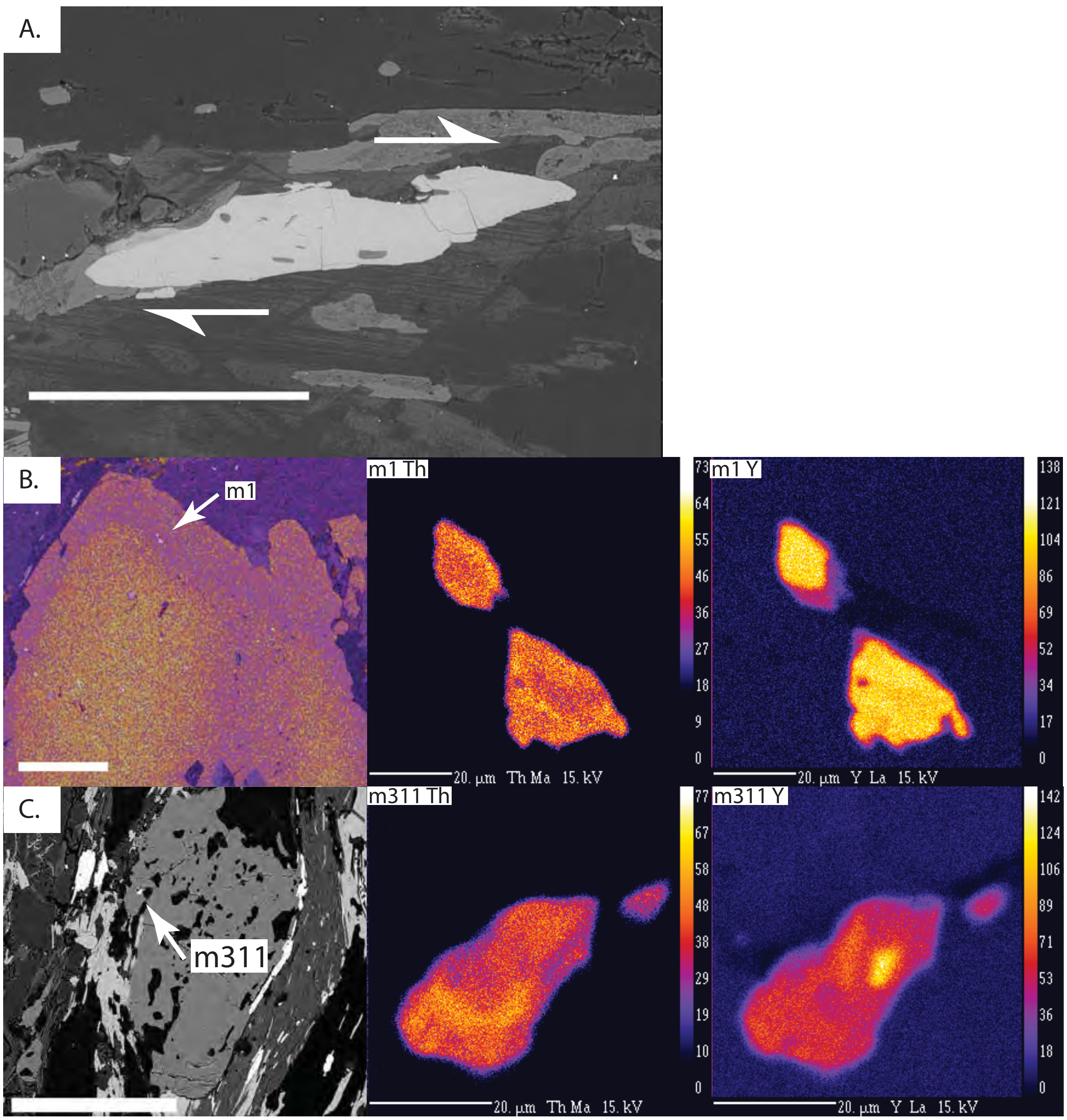

This is a preprint, the final version is subject to change, of the American Mineralogist (MSA)
Cite as Authors (Year) Title. American Mineralogist, in press.
(DOI will not work until issue is live.) DOI: http://dx.doi.org/10.2138/am-2016-5482

Bosbyshell et al. Figure 12

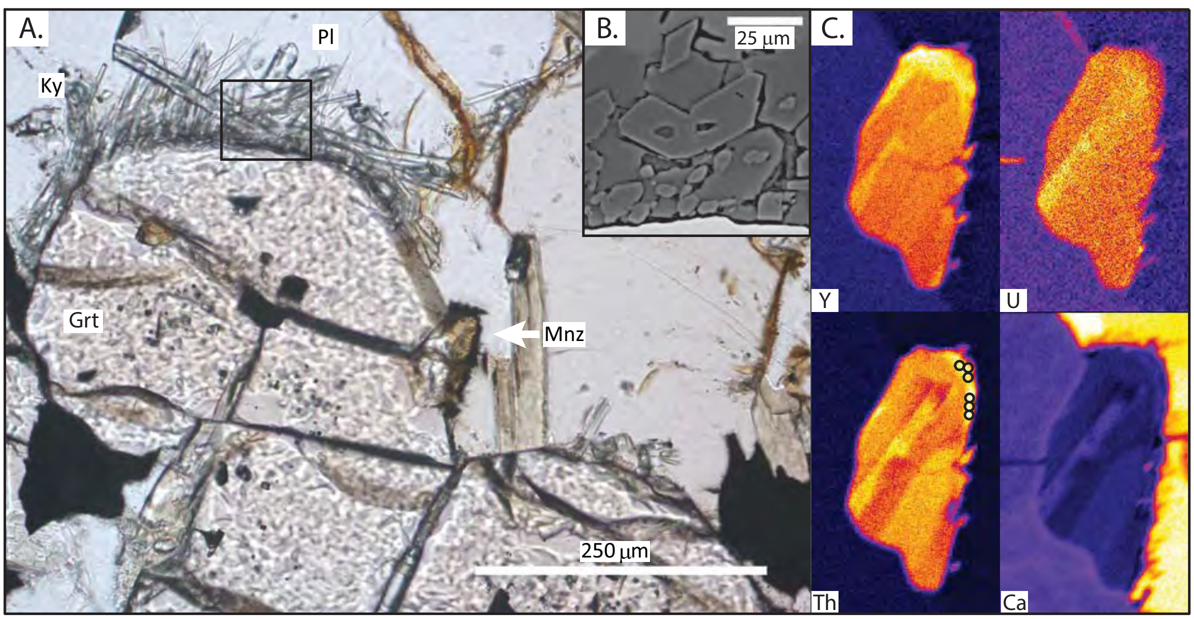

This is a preprint, the final version is subject to change, of the American Mineralogist (MSA)
Cite as Authors (Year) Title. American Mineralogist, in press.
(DOI will not work until issue is live.) DOI: http://dx.doi.org/10.2138/am-2016-5482

Bosbyshell et al. Figure 13

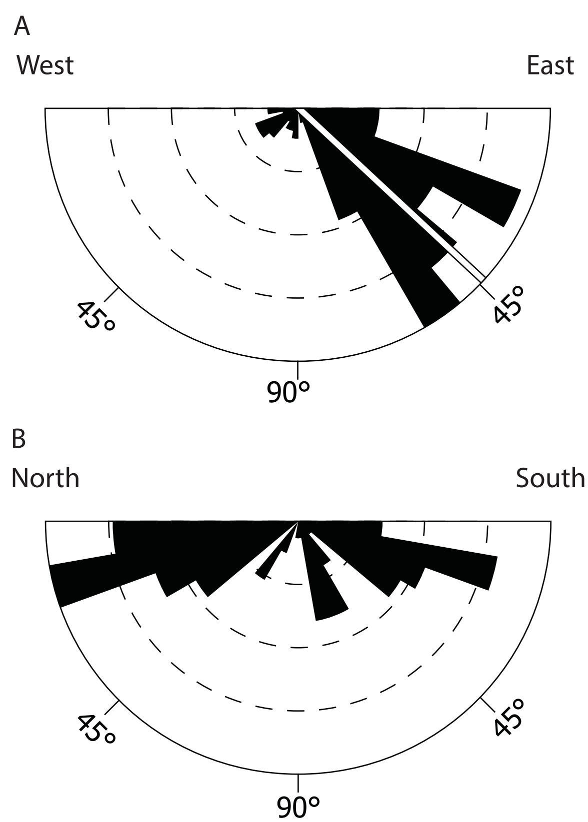

Bosbyshell et al. Figure 14

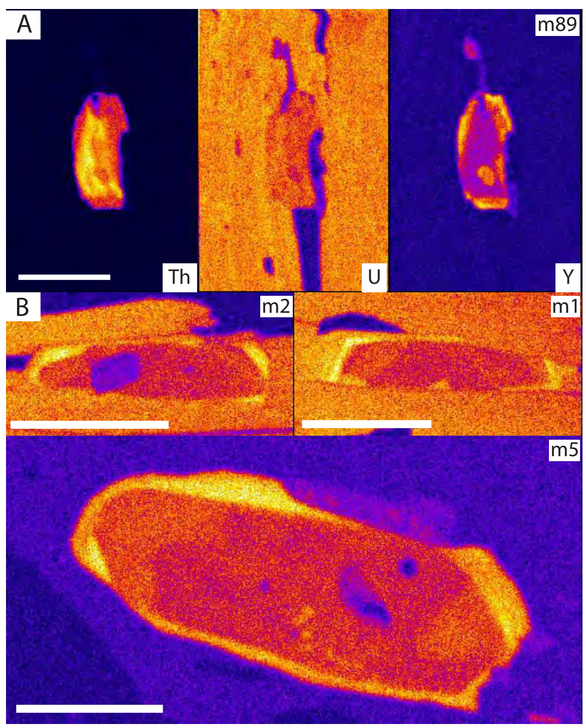

This is a preprint, the final version is subject to change, of the American Mineralogist (MSA)
Cite as Authors (Year) Title. American Mineralogist, in press.
(DOI will not work until issue is live.) DOI: http://dx.doi.org/10.2138/am-2016-5482

Bosbyshell et al. Figure 15

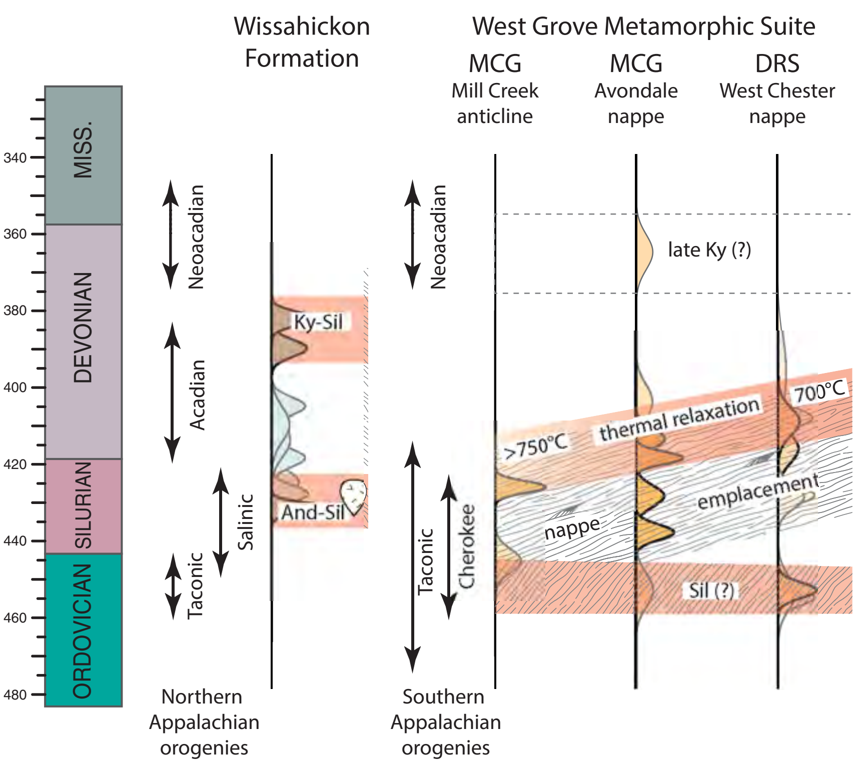

Bosbyshell et al. Figure 16